Monthly Notices of the ROYAL ASTRONOMICAL SOCIETY

MNRAS **519,** 4325–4343 (2023) https://doi.org/10.1093/mnras/stac3614
Advance Access publication 2022 December 12

Beyond the linear tide: impact of the non-linear tidal response of neutron stars on gravitational waveforms from binary inspirals

Hang Yu [1]★ Nevin N. Weinberg [2] Phil Arras [3] James Kwon[4] and Tejaswi Venumadhav[4,5]

[1]*Kavli Institute for Theoretical Physics, University of California at Santa Barbara, Santa Barbara, CA 93106, USA*
[2]*Department of Physics, University of Texas at Arlington, Arlington, TX 76019, USA*
[3]*Department of Astronomy, University of Virginia, P.O. Box 400325, Charlottesville, VA 22904, USA*
[4]*Department of Physics, University of California at Santa Barbara, Santa Barbara, CA 93106, USA*
[5]*International Centre for Theoretical Sciences, Tata Institute of Fundamental Research, Bangalore 560089, India*

Accepted 2022 December 5. in original form 2022 November 21

ABSTRACT

Tidal interactions in coalescing binary neutron stars modify the dynamics of the inspiral and hence imprint a signature on their gravitational wave (GW) signals in the form of an extra phase shift. We need accurate models for the tidal phase shift in order to constrain the supranuclear equation of state from observations. In previous studies, GW waveform models were typically constructed by treating the tide as a linear response to a perturbing tidal field. In this work, we incorporate non-linear corrections due to hydrodynamic three- and four-mode interactions and show how they can improve the accuracy and explanatory power of waveform models. We set up and numerically solve the coupled differential equations for the orbit and the modes and analytically derive solutions of the system's equilibrium configuration. Our analytical solutions agree well with the numerical ones up to the merger and involve only algebraic relations, allowing for fast phase shift and waveform evaluations for different equations of state over a large parameter space. We find that, at Newtonian order, non-linear fluid effects can enhance the tidal phase shift by $\gtrsim 1$ radian at a GW frequency of 1000 Hz, corresponding to a $10\% - 20\%$ correction to the linear theory. The scale of the additional phase shift near the merger is consistent with the difference between numerical relativity and theoretical predictions that account only for the linear tide. Non-linear fluid effects are thus important when interpreting the results of numerical relativity and in the construction of waveform models for current and future GW detectors.

Key words: gravitational waves – methods: analytical – (stars:) binaries (including multiple): close – stars: neutron.

1 INTRODUCTION

Neutron stars (NSs) are astrophysical laboratories for physics at extreme conditions. An NS in a coalescing binary driven by gravitational wave (GW) radiation can be tidally deformed, and the deformation and the associated change in the binary dynamics leave imprints in the associated GW waveform. These effects have been incorporated into the analysis of GW170817, the first binary NS (BNS) event detected by GW observation (LIGO Scientific Collaboration, Virgo Collaboration & et al. 2017, 2019a), and enabled valuable constraints on the supranuclear equation of state (EoS) (LIGO Scientific Collaboration, Virgo Collaboration & et al. 2018). With more BNSs detected (LIGO Scientific Collaboration, Virgo Collaboration & et al. 2020) and even more to be expected, especially when future GW detectors like the Einstein Telescope (Hild et al. 2010; Sathyaprakash et al. 2012) and the Cosmic Explorer (Abbott et al. 2017; Evans et al. 2021) become operational, it is imperative to develop more sophisticated theoretical waveform models to maximize the information we can extract.

Tidal effects within BNS systems can, in principle, lead to rich phenomenology. The dominant effect is the interaction between the tidal field and the fundamental mode (f-mode) of the NS, which characterizes the star's large-scale deformation of the NS. This was first studied in the adiabatic limit, i.e. assuming that the tidal driving frequency is much smaller than the eigenfrequency of the f-mode (Lai, Rasio & Shapiro 1993, 1994a, b; Flanagan & Hinderer 2008; Bini & Damour 2014; Bernuzzi et al. 2015). In this limit, the tidal response can be well characterized by a single coefficient known as the Love number k_2 (or equivalently, the NS deformability $\Lambda = 2k_2R^5/3$ with R the radius of the NS; Binnington & Poisson 2009; Damour & Nagar 2009; Hinderer et al. 2010). However, the driving frequency can become comparable to the eigenfrequency of the f-mode near the merger, leading to important corrections to the tidal response due to finite-frequency effects (Hinderer et al. 2016; Steinhoff et al. 2016; Andersson & Pnigouras 2021). If the NS spins significantly in a retrograde manner with respect to the orbit, the f-mode can even be resonantly excited (Ho & Lai 1999; Ma, Yu & Chen 2020; Steinhoff et al. 2021).

At a more detailed level, as the orbit decays due to GW radiation, the tide can resonantly excite gravity modes (g-modes; Lai 1994; Reisenegger & Goldreich 1994; Yu & Weinberg 2017a, b; Kuan, Suvorov & Kokkotas 2021a, b) and interface modes (Tsang et al. 2012; Pan et al. 2020; Passamonti, Andersson & Pnigouras 2021) within the NSs; if the stars are spinning about their individual axes, inertial modes can also be resonantly excited (Ho & Lai 1999;

★ E-mail: hang.yu2@montana.edu

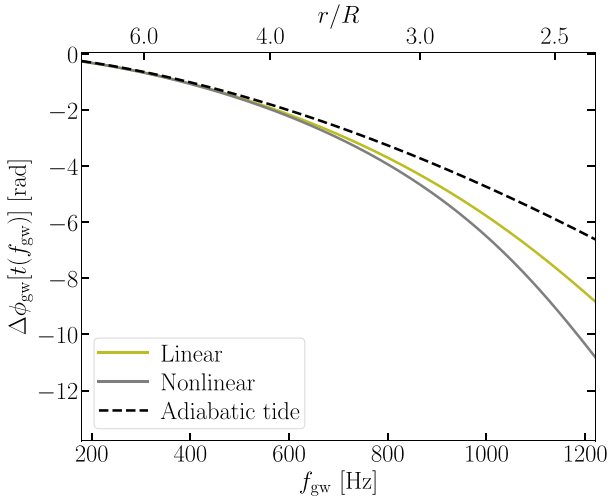

Figure 1. Tidal phase shift due to an NS with $M = 1.3\,\mathrm{M}_\odot$, $R = 12\,\mathrm{km}$, and $k_2 = 0.26$. The companion is assumed to be a point particle with $M' = M$. We show the result including just the linear tide (olive curve) and when including non-linear fluid effects (grey curve). As a reference, the phase shift in the adiabatic limit is shown in the black-dashed line using expressions in Hinderer et al. (2010). The non-linear tide corrects the phase by $\gtrsim 1$ rad at $f_{\rm gw} > 1000\,\mathrm{Hz}$ (at Newtonian order). This is consistent with the discrepancy between analytical results with linear tides and numerical relativity (Hinderer et al. 2016).

Flanagan & Racine 2007; Xu & Lai 2017; Poisson 2020; Gupta, Steinhoff & Hinderer 2021; Ma, Yu & Chen 2021).

An accurate waveform model incorporating these dynamics is essential to properly use the tidal signature in the data to constrain the EoS (Read et al. 2009; Damour, Nagar & Villain 2012; Del Pozzo et al. 2013; Lackey & Wade 2015; Andersson & Ho 2018; Landry & Essick 2019; Matas et al. 2020; Pratten, Schmidt & Williams 2022). If the NS EoS is known, BNS events can be further used to test the theory of general relativity (GR; Saffer & Yagi 2021) and probe the cosmological expansion history (Messenger & Read 2012).

Previous theoretical tidal models show good agreement with numerical relativity (Hotokezaka et al. 2015; Foucart et al. 2019) for most of the binary's inspiral; however, there is a discrepancy of about 1 radian between the phases of analytical and numerical waveforms near the final merger (Hinderer et al. 2016; Nagar et al. 2018; Steinhoff et al. 2021) whose origin is yet unclear. Understanding the discrepancy would be of great theoretical interest for correctly interpreting the results of numerical relativity and constraining the binary dynamics in the highly relativistic regime. Moreover, it would enable us to construct accurate waveform templates for efficient parameter space exploration and data analysis.

In this work, we investigate the effects of the non-linear tide including interactions among NS modes as well as between modes and the non-linear tidal driving. Our main result is illustrated in Fig. 1. Here, we present the tidal phase shift of the GW waveform. The olive curve shows the result obtained using the linear dynamical tide theory and the grey curve includes the effects of the non-linear tide, which we will examine in detail in this work. In particular, the non-linear tide creates an additional phase shift of $\mathcal{O}(1)$ rad near the merger compared to the linear result, which is consistent with the discrepancy between previous theoretical and numerical works. This suggests that non-linear effects could be (at least in part) the cause of the discrepancy, and that they should be a key component of future waveform modelling.

Table 1. Coupling coefficients of the $\Gamma = 2$ polytrope model assumed in our study. The $l = 2$ f-modes in our model have $\omega_a = 1.2\omega_0 \simeq 1.95 \times 10^3$ Hz.

Quantity	(l_a, m_a)	n_a	Value
I_a	(2, ±2 or 0)	0	0.32
	(2, ±2 or 0)	1	-5.5×10^{-3}
J_{ablm}	(2,+2), (2,–2), (2,0)	0, 0, tide	–0.21(=J_2)
	(2,0), (2,0), (2,0)	0, 0, tide	0.21(=J_0)
	(2,+2), (2,–2), (2,0)	0, 1, tide	1.2×10^{-3}
κ_{abc}	(2,+2), (2,–2), (2, 0)	0, 0, 0	–0.45(=κ_2)
	(2, 0), (2, 0), (2, 0)	0, 0, 0	0.45(=κ_0)
	(2,+2), (2,–2), (2, 0)	0, 0, 1	−0.04
	(2,+2), (2,+2), (4,-4)	0, 0, 0	0.19
	(2,+2), (2,–2), (4, 0)	0, 0, 0	0.02
	(2,+2), (2,–2), (0, 0)	0, 0, 1	0.88
	(2, 0), (2, 0), (4, 0)	0, 0, 0	0.13
	(2, 0), (2, 0), (0, 0)	0, 0, 1	0.88
η_{abcd}	(2,+2), (2,+2), (2,–2), (2,–2)	0,0,0,0	−1.75(=η_{22})
	(2,+2), (2,–2), (2, 0), (2, 0)	0,0,0,0	−0.89(=η_{20})
	(2, 0), (2, 0), (2, 0), (2, 0)	0,0,0,0	−0.89

We note that our result is greater than the prior estimate of non-linear hydrodynamic corrections in Hinderer et al. (2010) for a few reasons. First, we perform a first-principle calculation of the non-linear coupling following Weinberg et al. (2012) and find that the coupling strength is greater than the estimation of Hinderer et al. (2010) (see later in Table 1). Also, Hinderer et al. (2010) ignored the non-linear part of the tidally induced NS mass quadrupole $Q^{ij}_{\rm ns}$ [see equation (C1)] and therefore did not account for the non-linear tidal driving [i.e. the term $\propto U_{ablm}$ in equation (2)]. Lastly, the finite-frequency correction to the f-mode was underestimated in Hinderer et al. (2010) (though its significance was later realized in Hinderer et al. 2016; Steinhoff et al. 2016). Our study finds that the major non-linear hydrodynamic correction is in fact a shift to the f-mode's frequency, which strengthens the mode's finite-frequency response [see equation (20) and Fig. 3]. These reasons explain the difference between our result and the estimate of Hinderer et al. (2010).

Before we proceed, we also note that the non-linear tide we investigate here is different from the non-linear pg-instability (Weinberg, Arras & Burkart 2013; Venumadhav, Zimmerman & Hirata 2014; Essick, Vitale & Weinberg 2016; Weinberg 2016; LIGO Scientific Collaboration et al. 2019b). The pg-instability describes the coupling between the tide and high-order pressure and gravity modes and it modifies the orbital evolution by fluid dissipation. In contrast, our focus in this work will be on the interactions among low-order modes as well as their non-linear couplings with the tidal potential. The interaction is conservative when the GW radiation is ignored.

In the rest of the paper, we will explain the details leading to Fig. 1. In particular, we will first introduce the equations governing the evolution of NS modes in Section 2. Approximate solutions of the modes will be presented in Sections 2.1 and 2.2 at the linear and non-linear orders, respectively. We will then describe the evolution of the orbit in Section 3 including both tidal back reaction and radiation reaction. This is followed by analytical solutions to the system's equilibrium configuration in Section 4. Lastly, we conclude and discuss our results in Section 5. The appendices contain a section with a simple intuitive explanation of non-linear corrections to the tide (Appendix A), as well as important technical details relevant to the calculations (Appendices B–D). Throughout the paper, we will use geometrical units with $G = c = 1$.

2 DYNAMICS OF THE MODES

In this section, we study the motion of perturbed fluid in an NS in terms of the NS's eigenmodes. We derive a set of differential

equations governing the amplitude of each mode that include leading-order non-linear interactions corresponding to three-mode and four-mode couplings. This set of equations can be integrated numerically or solved analytically with approximations (Sections 2.1 and 2.2). When combined with the equations governing the orbit (Section 3), we can obtain a complete description of the system.

Suppose $\boldsymbol{\xi}$ is the Lagrangian displacement of a tidally perturbed NS. We perform a phase space decomposition following Schenk et al. (2002) as

$$\begin{bmatrix}\boldsymbol{\xi}(\boldsymbol{x},t)\\ \dot{\boldsymbol{\xi}}(\boldsymbol{x},t)\end{bmatrix} = \sum_a c_a(t)\begin{bmatrix}\boldsymbol{\xi}_a(\boldsymbol{x})\\ -i\omega_a\boldsymbol{\xi}_a(\boldsymbol{x})\end{bmatrix}, \tag{1}$$

where a mode a is labelled by two angular quantum numbers (l_a, m_a) (for its angular pattern governed by the spherical harmonic $Y_{l_a m_a}$), one radial order n_a (with $n_a = 0$ for the f-mode and $n_a > 0$ for p-modes), and a sign of its eigenfrequencies (either positive or negative). Following Schenk et al. (2002), one can show that a mode with ($-\omega_a$, $-m_a$) is the complex conjugate of the mode with (ω_a, m_a). When we discuss a mode in the subsequent text, we will restrict to the positive frequency one if we do not explicitly mention its sign. In our equations, on the other hand, the summations run over all the modes including both signs of eigenfrequencies. We will add $\omega_a > 0$ above the summation symbol if we explicitly pair a mode and its complex conjugate first and then restrict the summation over only half of the modes.

Consider the leading-order non-linear effect, the conservative part of the amplitude equation of a mode a is (Weinberg et al. 2012; Venumadhav et al. 2014; Weinberg 2016)

$$\dot{c}_a + i\omega_a c_a = i\omega_a\left[U_a + \sum_{b,lm} U^*_{ablm}c^*_b + \sum_{bc}\kappa_{abc}c^*_b c^*_c + \sum_{bcd}\eta_{abcd}c^*_b c^*_c c^*_d\right], \tag{2}$$

where the left-hand side describes a harmonic oscillator and the right-hand side describes various driving terms, which will be described in detail shortly. In principle, there will also be a four-mode counterpart to U_{ablm}, yet we argue in Appendix B that it should be subdominant and would not significantly modify the results obtained in this study. To obtain the above equation, we normalize each mode so that

$$2\omega_a^2\int \mathrm{d}^3x\,\rho\boldsymbol{\xi}^*_a\cdot\boldsymbol{\xi}_b = \delta_{ab}E_0, \tag{3}$$

where $E_0 = M^2/R$. Dissipation due to, e.g. Urca reactions is estimated to be small (Arras & Weinberg 2019; Alford et al. 2021) and hence ignored in our analysis (but see Section 3 and Appendix C for the damping due to GW radiation). In particular, the term U_a describes the linear tidal driving and is given by

$$U_a = \frac{M'}{M}W_{l_a m_a}I_{alm}\left(\frac{R}{r}\right)^{l_a+1}e^{-\mathrm{i}m_a\phi} = V_a e^{-\mathrm{i}m_a\phi}, \tag{4}$$

where r and ϕ are, respectively, the orbital separation and phase, and $W_{lm} = 4\pi(2l+1)^{-1}Y_{lm}(\pi/2, 0)$. For the $l = 2$ tide, the non-zero values of W_{lm} are $W_{22} = W_{2-2} = \sqrt{3\pi/10}$ and $W_{20} = -\sqrt{\pi/5}$. We used for the spatial coupling $I_{alm} = I_a\delta_{ll_a}\delta_{mm_a}$, where I_a is the linear tidal coupling coefficient (also known as the tidal overlap),

$$I_a = \frac{1}{MR^{l_a}}\int \mathrm{d}^3x\,\rho\boldsymbol{\xi}^*_a\cdot\nabla(r^{l_a}Y_{l_a m_a}). \tag{5}$$

It is evaluated using equation (A15) in Weinberg et al. (2012). Under the adiabatic limit $\Omega \equiv \dot{\phi} \ll \omega_a$, I_a of the $l_a = 2$ f-mode is related to the Love number k_2 by (Appendix C; see also, e.g. Andersson & Pnigouras 2020; Passamonti, Andersson & Pnigouras 2022)

$$k_2 \simeq \frac{4\pi}{5}I_a^2. \tag{6}$$

where we ignore other modes' contributions to the Love number since they are negligible for an NS. The U_{ablm} term is due to non-linear tidal driving. We write

$$U_{ablm} = \frac{M'}{M}W_{lm}J_{ablm}\left(\frac{R}{r}\right)^{l+1}e^{-im\phi} = V_{ablm}e^{-im\phi} \tag{7}$$

where the coefficient J_{ablm} is defined as

$$J_{ablm} = \frac{1}{MR^l}\int \mathrm{d}^3x\,\rho\boldsymbol{\xi}_a\cdot\left(\boldsymbol{\xi}_b\cdot\nabla\right)\nabla(r^lY_{lm}), \tag{8}$$

and we compute it numerically according to equation (A23) of Weinberg et al. (2012). The κ_{abc} term describes the coupling between three eigenmodes of the star and it is computed according to equations (A55)-(A62) of Weinberg et al. (2012). Lastly, the η_{abcd} term describes the four-mode coupling and its computation is described by appendix C in Weinberg (2016). For f-modes, the perturbed gravity is significant and the Cowling approximation (Cowling 1941) should not be adopted. We derive in Appendix D the additional contributions to η_{abcd} due to terms involving perturbed gravity. We find that they can modify the results of Weinberg (2016) made under the Cowling approximation by 70 per cent for f-modes.

We present numerical values for key coupling coefficients in Table 1.[1] In our study, we assume that the background NS is described by a $P \propto \rho^\Gamma$ polytrope with $\Gamma = 2$. We set its mass to $M = 1.3\,\mathrm{M}_\odot$ and radius to $R = 12\,\mathrm{km}$, corresponding to a compactness $M/R = 0.16$. Other natural units of this model are $E_0 = 3.7\times10^{53}$ erg and $\omega_0/2\pi = 1.6\times10^3$ Hz where $\omega_0^2 \equiv M/R^3$. The modes are computed using stellar oscillation code GYRE (Townsend & Teitler 2013; Townsend, Goldstein & Zweibel 2018). We further assume that the background NS is non-spinning, neutrally stratified (with the Brunt-Väisälä frequency $\mathcal{N} = 0$, i.e. no g-modes in our model), and under *Newtonian* hydrostatic equilibrium. While we include the quadrupole GW radiation, other GR effects will be ignored in the current study for simplicity.

For future convenience, we introduce $C_a = c_a\exp[im_a\phi]$. Prior to resonance, c_a oscillates at the same rate as the driving potential at $m_a\Omega$, where $\Omega = \pi f_{\mathrm{gw}}$ with f_{gw} the GW frequency. Thus, by using C_a, we factor out the fast-oscillating part of c_a and the remaining temporal changes are due to the GW-driven orbital decay only.

In our numerical calculations, we include the $l = 2$, $m = 0, \pm2$ f-modes, which dominate the linear tidal responses. The p-modes have little contribution to the result because of their small overlap with the tidal potential (Table 1 compares the f-mode and the $n_a = 1$ p-mode). When computing the non-linear tidal driving U_{ablm}, we focus on the contributions from $l = 2$. We further include the first $l = 0$ (radial) mode and the $l = 4$, $m = 0, \pm2, \pm4$ f-modes, which can couple with a pair of $l = 2$ f-modes via the three-mode coupling channel. They are critical in determining the anharmonic frequency shift of an (l, m) = (2, 2) *free* oscillator (Yu, Weinberg & Arras 2021, 2022) together with the four-mode couplings among the $l = 2$ modes. Yet, as we will see in the later discussions, because the l

[1]Note that when normalizing the eigenfunction of each mode by a constant, we have a freedom in choosing the sign. Changing the sign convention will change the signs of I_a and κ_{abc}, yet the physical results (see, e.g. Section 2.2 below) will not be affected because they depend on the product $\kappa_{abc}I_a$. When J_{ablm} appears alone, it will be due to a mode coupling with its complex conjugate, so it is not affected by the choice of the normalization sign, either.

$= 2$ modes are *continuously forced* by the tidal potential (thus not freely oscillating) in our case, the leading-order non-linear correction comes from their mutual couplings and the anharmonic effect of a free oscillator is small. An $l = 3$, $|m| = 1$ or 3 mode with $W_{3m} \neq 0$ cannot couple with a pair of $l = 2$ modes as it violates the angular selection rule (Weinberg et al. 2012) and therefore does not contribute to the non-linear tide at the leading order. Since the linear $l = 3$ tide has been well studied (Hinderer et al. 2016), we ignore it here for simplicity.

2.1 Linear solution

Let b_a be the solution of the linear problem and define $B_a = b_a \exp[im_a\phi]$. By equation (2), the equation for B_a is given by

$$\dot{B}_a + i(\omega_a - m_a\Omega)B_a = i\omega_a V_a. \tag{9}$$

Since B_a varies slowly in time prior to resonance (i.e. when $m_a\Omega < \omega_a$), we can obtain a zeroth-order solution by ignoring the $\dot{B}_a$ term, which leads to

$$B_a^{(0)} = \frac{\omega_a}{\omega_a - m_a\Omega} V_a. \tag{10}$$

The zeroth-order solution is then plugged back into equation (9) to obtain the first-order correction $B_a^{(1)}$. Again dropping the $\dot{B}_a^{(1)}$ term, we have

$$\begin{aligned} B_a^{(1)} &= \frac{i}{(\omega_a - m_a\Omega)} \dot{B}_a^{(0)} \\ &= \frac{i\omega_a}{(\omega_a - m_a\Omega)^2} \left[\frac{2}{3}(l+1) + \frac{m_a\Omega}{\omega_a - m_a\Omega}\right] \frac{\dot{\Omega}}{\Omega} V_a. \end{aligned} \tag{11}$$

The solution of B_a is thus obtained as $B_a = B_a^{(0)} + B_a^{(1)} + ...$

2.2 Including non-linear effects

We now consider a system including the leading-order non-linear corrections. In this subsection, we will let mode (a, b, c), respectively, have $(l_a, m_a) = (2, 2)$, $(l_b, m_b) = (2, -2)$, and $(l_c, m_c) = (2, 0)$. In other words, we let mode a (b) be the prograde (retrograde) mode specifically in this section. We consider their mutual couplings as well as the coupling with the $l = 2$ tidal potential (via the U_{ablm} term). This set of interactions covers all the non-linear corrections to the linear mode amplitude formally at the $(R/r)^3$ order. To make the problem explicit, we write out all the allowed couplings

$$\begin{aligned} \dot{C}_a + i(\omega_a - m_a\Omega)\, C_a &= i\omega_a[V_a + V_{aa^*20}C_a \\ &\quad + V_{ab20}C_b^* + V_{ac2-2}C_c^* + V_{ac^*2-2}C_c \\ &\quad + 2\kappa_{aa^*c}C_aC_c^* + 2\kappa_{aa^*c^*}C_aC_c \\ &\quad + 2\kappa_{abc}C_b^*C_c^* + 2\kappa_{abc^*}C_b^*C_c], \end{aligned} \tag{12}$$

$$\begin{aligned} \dot{C}_b + i(\omega_b - m_b\Omega)\, C_b &= i\omega_b[V_b + V_{ab20}C_a^* \\ &\quad + V_{bb^*20}C_b + V_{bc22}C_c^* + V_{bc^*22}C_c \\ &\quad + 2\kappa_{abc}C_a^*C_c^* + 2\kappa_{abc^*}C_a^*C_c \\ &\quad + 2\kappa_{bb^*c}C_bC_c^* + 2\kappa_{bb^*c^*}C_bC_c], \end{aligned} \tag{13}$$

$$\begin{aligned} \dot{C}_c + i\omega_c C_c &= i\omega_c[V_c + V_{ac2-2}C_a^* + V_{a^*c22}C_a \\ &\quad + V_{bc22}C_b^* + V_{b^*c2-2}C_b + V_{cc^*20}C_c + V_{cc20}C_c^* \\ &\quad + 2\kappa_{aa^*c}C_aC_a^* + 2\kappa_{bb^*c}C_bC_b^* \\ &\quad + 2\kappa_{abc}C_a^*C_b^* + 2\kappa_{a^*b^*c}C_aC_b \\ &\quad + \kappa_{ccc}C_c^*C_c^* + \kappa_{cc^*c^*}C_cC_c + 2\kappa_{ccc^*}C_cC_c^*]. \end{aligned} \tag{14}$$

Furthermore, we note that both κ_{abc} and J_{ablm} are symmetric with respect to permutations of the mode indices. Moreover, the $l = 2$ modes have the same eigenfrequency ($\omega_a = \omega_b = \omega_c > 0$) and the same reduced eigenfunction (after separating out the angular part described by each mode's specific spherical harmonic). We thus have

$$\begin{aligned} V_a = V_b = V_2, \quad V_c &= V_0; \\ V_{aa^*20} &= \text{similar terms} = V_{20}; \\ V_{ac2-2} &= \text{similar terms} = V_{22}; \\ V_{cc20} &= \text{similar terms} = V_{00}; \\ J_{ab20} = J_{ac2-2} &= \text{similar terms} = J_2; \\ J_{cc20} &= \text{similar terms} = J_0; \\ \kappa_{abc} &= \text{similar terms} = \kappa_2; \\ \kappa_{ccc} &= \text{similar terms} = \kappa_0. \end{aligned}$$

Numerically, we see from Table 1 that

$$J_2 = -J_0 = -0.21 \text{ and } \kappa_2 = -\kappa_0 = -0.45. \tag{15}$$

The difference between J_2 and J_0 (and similarly between κ_2 and κ_0) is purely due to the angular overlap. Therefore, $J_2 = -J_0$ and $\kappa_2 = -\kappa_0$ hold independent of the choice of EoS.

The non-linear terms in, e.g. the right-hand side of equation (12) have two effects. The terms containing C_a correspond to an effective shift of the mode's eigenfrequency ω_a while terms that are independent of C_a modify the driving potential. Using the linear solutions obtained in Section 2.1, we can define the leading-order frequency shift[2]

$$\begin{aligned} \frac{\Delta\omega_a}{\omega_a} &= -V_{20} - 4\kappa_2 \mathrm{Re}[B_c], \\ &= \sqrt{\frac{\pi}{5}}\,(J_2 + 4\kappa_2 I_a)\, R^3 \frac{M'}{M}\frac{\Omega^2}{M_\mathrm{t}}, \end{aligned} \tag{16}$$

where $M_\mathrm{t} = M' + M$. Note $\Delta\omega_a/\omega_a < 0$ (Table 1). The origin of this frequency shift and its sign can be understood with a toy model described in Appendix A. Meanwhile, the modifications of the driving forces are

$$\begin{aligned} \Delta V_a &= V_{20}B_b^* + 2V_{22}\mathrm{Re}[B_c] + 4\kappa_2 \mathrm{Re}[B_c]B_b^*, \\ &\simeq -\frac{\pi}{5}\sqrt{\frac{3}{2}}\left[2J_2 I_a + \frac{\omega_a}{\omega_a + 2\Omega}\,(J_2 + 4\kappa_2 I_a)\, I_a\right] \\ &\quad \times R^6 \frac{M'^2}{M^2}\frac{\Omega^4}{M_\mathrm{t}^2}, \end{aligned} \tag{17}$$

[2]Note that the partial cancellation between J_{ablm} and $2\kappa_{abc}I_c$ described in section 5.2 of Weinberg et al. (2012) is not significant in our case. The partial cancellation arises when using method 2 in section 2.1.2 of Weinberg et al. (2012) or considering the linear tide coupling with two eigenmodes. In this description, the inhomogeneous piece of the linear tide will lead to an extra piece in the three-mode coupling that cancels the contribution to J_{ablm} from the horizontal mode displacements [the term containing $a_l b_l$ in equation (A23) of Weinberg et al. (2012)]. This cancellation is significant when considering the coupling with high-order g-modes whose displacements are predominantly horizontal but less significant for the coupling with f-modes whose motions are mainly radial. Moreover, we adopt method 1 in section 2.1.1 of Weinberg et al. (2012) and describe the tide in terms of eigenmodes. This avoids the inhomogeneous piece in the coupling coefficient; yet, we will be subject to truncation errors due to ignoring high-order ($|n_a| \geq 1$) modes. Nevertheless, from Table 1 we see that I_a, J_{ablm}, and κ_{abc} are all strongly dominated by the f-modes (one or two orders of magnitudes above the values involving p-modes). The g-modes, when present, also have small contributions to the tidal response (see, e.g. Lai 1994). Consequently, the truncation error due to ignoring high-order modes is expected to be small.

$$\Delta V_b = V_{20} B_a^* + 2V_{22}\mathrm{Re}[B_c] + 4\kappa_2 \mathrm{Re}[B_c] B_a^*,$$
$$\simeq -\frac{\pi}{5}\sqrt{\frac{3}{2}}\left[2J_2 I_a + \frac{\omega_a}{\omega_a - 2\Omega}(J_2 + 4\kappa_2 I_a) I_a\right]$$
$$\times R^6 \frac{M'^2}{M^2}\frac{\Omega^4}{M_t^2}, \tag{18}$$

$$\Delta V_c = 2\mathrm{Re}\,[V_{22} B_a + V_{22} B_b + V_{00} B_c +$$
$$+ \kappa_2 |B_a|^2 + \kappa_2 |B_b|^2 + 2\kappa_2 B_a B_b + 2\kappa_0 |B_c|^2]$$
$$\simeq 2\left[\frac{3\pi}{10}\frac{2\omega_a^2}{\omega_a^2 - 4\Omega^2} I_a \left(J_2 + \frac{2\omega_a^2}{\omega_a^2 - 4\Omega^2}\kappa_2 I_a\right)\right.$$
$$\left. + \frac{\pi}{5} I_a (J_0 + 2\kappa_0 I_a)\right] R^6 \frac{M'^2}{M^2}\frac{\Omega^4}{M_t^2}. \tag{19}$$

We can thus obtain the amplitude of each mode as

$$C_{a,b} = \frac{\omega_a}{\omega_a + \Delta\omega_a - m_{a,b}\Omega}\left(V_2 + \Delta V_{a,b}\right), \tag{20}$$

$$C_c = V_0 + \Delta V_c, \tag{21}$$

with the linear potentials given by

$$V_{2(\mathrm{or}\,0)} = W_{22(\mathrm{or}\,20)} \frac{M'}{M} I_a R^3 \frac{\Omega^2}{M_t}. \tag{22}$$

In the equations above, we have used the point-particle (PP) Keplerian orbit to replace r^3 by M_t/Ω^2. As we will see in Section 4, the errors introduced by using the Keplerian orbit are of higher order than the leading-order non-linear tide we consider here and can thus be dropped.

The above equations show that to get the leading-order non-linear corrections due to hydrodynamics, we only need to compute two additional EoS-dependent coupling coefficients, κ_2 and J_2 [see the discussion below equation (15)], which describe, respectively, the coupling between three f-modes and the coupling between two f-modes and the tidal driving potential. They can be determined from an isolated NS, similar to the determination of I_a (or effectively, the Love number k_2). Once the coupling coefficients are known, we can then express the mode amplitude in terms of the orbital frequency Ω, allowing them to be easily evaluated with algebraic relations only.

Fig. 2 shows that the analytical approximation computed using equations (16)–(21) is in good agreement with the full numerical solution to the differential equations [equation (2) coupled to equations (25)–(26)] up to the merger defined as where the NS's perturbed surface would contact the companion ($r \simeq 2.3R$ or $f_{\rm gw} \simeq 1250\,$Hz). The simple expressions we obtained under only one iteration of perturbation holding well is a consequence of the fact that the next-order perturbation from the three-mode terms cancels partially with the four-mode couplings included in equation (2). Without this cancellation, the system would evolve into an unphysical amplitude instability as described in appendix D of Wu (1998). We will illustrate this point further in Appendix B.

It is interesting to note that the fractional correction to the mode amplitude,

$$\frac{C_a}{B_a} - 1 \simeq -\frac{\Delta\omega_a}{\omega_a - m_a\Omega} + \frac{\Delta V_a}{V_a}, \tag{23}$$

is greater than $(R/r)^3 \propto f_{\rm gw}^2$ because of the finite frequency response of the modes. This is illustrated in Fig. 3. For the $|m| = 2$ modes (i.e. a and b), the main non-linear correction is the shift of the mode frequency towards lower values [grey curve in Fig. 3; see also equation (16) and Table (1), as well as the toy model in Appendix A]. The finite-frequency effect makes it greater than the correction to the driving potential $\propto \Delta V_a/V_a$ (olive curve) near the merger. Since we will need to sum over modes to get the physical tidal correction [see, e.g. equation (39)], it is also convenient to write the correction to the sum of the $|m| = 2$ modes as (focusing on the $\Delta\omega_a$ term)

$$\frac{C_a + C_b}{B_a + B_b} - 1 \simeq \frac{-2\omega_a^2}{\omega_a^2 - 4\Omega^2}\frac{\Delta\omega_a}{\omega_a}. \tag{24}$$

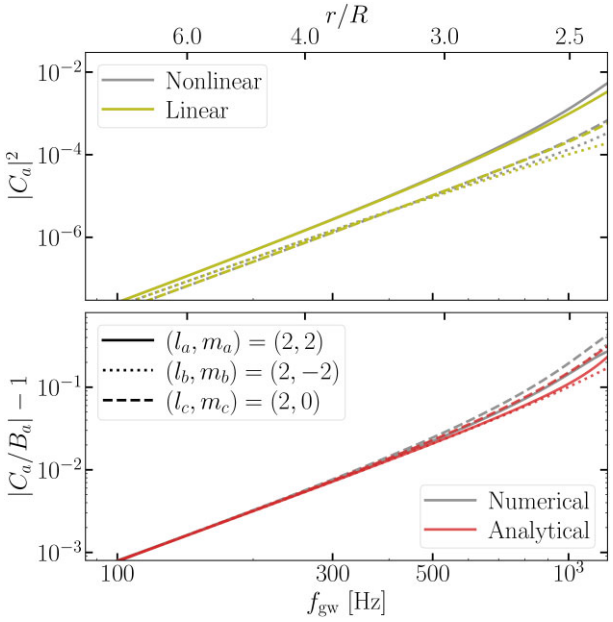

Figure 2. Top: energy of each mode in units of E_0 as a function of the GW frequency. Bottom: fractional corrections to the mode amplitude due to non-linear effects. The analytical approximation (red curves) obtained from equations (16)–(21) shows good agreement with the numerical solution (grey curves).

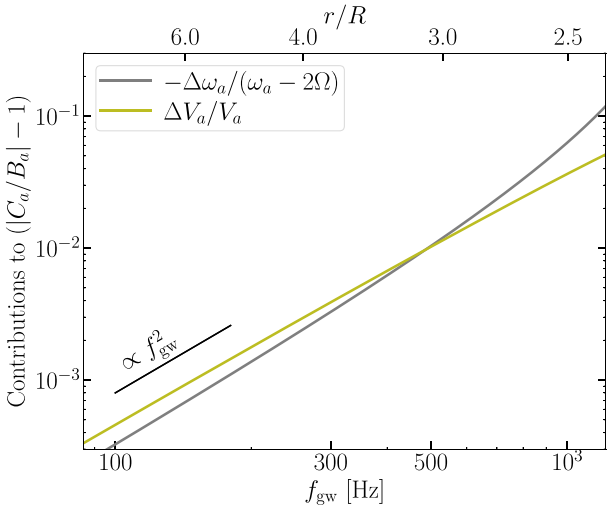

Figure 3. Comparison of different non-linear corrections to the mode amplitude [equation (23)]. For the $l_a = m_a = 2$, the dominant correction near the merger comes from the non-linear frequency shift $\Delta\omega_a$. As the frequency is lowered by non-linear interactions, the finite-frequency response of the mode is amplified, allowing the non-linear correction to be greater than $(R/r)^3 \propto f_{\rm gw}^2$.

For mode c, the correction is also amplified by the finite frequency response as ΔV_c contains terms like $B_a + B_b$ and $|B_a|^2 + |B_b|^2$. See equation (19).

We note that the frequency shift, equation (16), is different from the standard anharmonic behaviour of a *free* oscillator where the frequency shift is proportional to the energy of the mode (or $\propto f_{\rm gw}^4$ in the adiabatic limit; Landau & Lifshitz 1982; Kumar, Goldreich & Kerswell 1994; Yu et al. 2021). The anharmonicity originates from the oscillating mode deforming the background star (Lai 1996), which then creates a frequency shift of the mode. In contrast, in equation (16), the frequency shift goes as the amplitude (of a different mode) instead of the energy because of the continuous tidal forcing, and its origin can be understood from an intuitive toy model we present in Appendix A. While in our case we find the anharmonic effect to be subdominant, it could nonetheless be significant if the $l = m = 2$ f-mode has a significantly greater amplitude than the other $l = 2$ f-modes due to, e.g. a strong resonance with the orbit. The resonant excitation of the $m = 2$ mode could be possible if the NS is rapidly spinning (Ma et al. 2020; Steinhoff et al. 2021) or if the orbit is eccentric (Chirenti, Gold & Miller 2017; Parisi & Sturani 2018; Yang et al. 2018; Vick & Lai 2019; Yang 2019; Wang & Lai 2020). Thus, we also demonstrate the appearance of the standard anharmonic frequency shift in the modal picture we adopt in this study in Appendix B.

3 DYNAMICS OF THE ORBIT

Having described the evolution of the eigenmodes in the previous section, we now turn to the dynamics of the orbit including the effects due to tidal back-reactions and GW radiation.

The orbital evolution can be computed by (see, e.g. Flanagan & Racine 2007)

$$\ddot{r} - r\dot{\phi}^2 + \tfrac{(M+M')}{r^2} = g_r, \tag{25}$$

$$r\ddot{\phi} + 2\dot{r}\dot{\phi} = g_\phi, \tag{26}$$

where $g_r = g_r^{(\rm tide)} + g_r^{(\rm gw)}$ describes the radial acceleration acting on the orbit. It contains a conservative part due to the tidal back-reaction, $g_r^{(\rm tide)}$ and a dissipative part due to GW radiation, $g_r^{(\rm gw)}$. The tangential part, g_ϕ, can be decomposed in a similar way.

To derive the tidal back-reactions, we start from the interaction Hamiltonian given by (Weinberg et al. 2012; Yu, Weinberg & Fuller 2020)

$$H_{\rm int} = -E_0 \sum_{lm} \left[\sum_a^{\omega_a>0} (U_a c_a^* + U_a^* c_a) + \frac{1}{2} \sum_{ab}^{\omega_a>0} (U_{ab} c_a c_b + U_{ab}^* c_a^* c_b^*) \right]. \tag{27}$$

Note that we explicitly write out mode a and its complex conjugate a^*, so the summation runs over only modes with positive frequencies. In the non-linear tide term, the summation of mode b still runs over both signs of frequency.

From the Hamiltonian, we can derive the radial and tangential acceleration exerted by the mode on the orbit,

$$g_r^{(\rm tide)} = -\frac{1}{\mu}\frac{\partial H_{\rm int}}{\partial r} = -\frac{E_0}{\mu r} \times \sum_{lm} (l+1) \left[2 \sum_{a,\omega_a>0}^{m_a=m} {\rm Re}\left(U_a c_a^*\right) + \sum_{ab,\omega_a>0}^{m_a+m_b=-m} {\rm Re}\left(U_{ab} c_a c_b\right) \right], \tag{28}$$

$$g_\phi^{(\rm tide)} = -\frac{1}{\mu r}\frac{\partial H_{\rm int}}{\partial \phi} = \frac{E_0}{\mu r} \times \sum_{lm} m \left[2 \sum_{a,\omega_a>0}^{m_a=m} {\rm Im}\left(U_a c_a^*\right) + \sum_{ab,\omega_a>0}^{m_a+m_b=-m} {\rm Im}\left(U_{ab} c_a c_b\right) \right]. \tag{29}$$

The $g_{r,(\phi)}^{(\rm gw)}$ terms describe the Burke–Throne dissipation and they can be computed by (using tensor notations in a Cartesian coordinate with Einstein summation; Poisson & Will 2014)

$$g_{(\rm gw)}^i = -\frac{2}{5} r_j \frac{{\rm d}^5}{{\rm d}t^5} Q_{\rm tot}^{\langle ij \rangle}, \tag{30}$$

where r_j is the displacement vector of the orbit and $Q_{\rm tot}^{\langle ij \rangle}$ is the total mass quadrupole of the system, $Q_{\rm tot}^{\langle ij \rangle} = Q_{\rm orb}^{\langle ij \rangle} + Q_{\rm ns}^{\langle ij \rangle}$. The angular bracket denotes a symmetric, trace-free (STF) tensor. In other words, $Q_{\rm tot}^{\langle ij \rangle}$ is the linear sum of the orbital quadrupole, $Q_{\rm orb}^{\langle ij \rangle} = \mu r^i r^j - \mu r^2 \delta^{ij}/3$, and the NS quadrupole $Q_{\rm ns}^{\langle ij \rangle}$ (see Appendix C). In the PP limit, the Burke–Throne terms are given by (Flanagan & Racine 2007)

$$g_r^{(\rm gw,pp)} = \tfrac{16 M M'}{5 r^3} \dot{r} \left[\dot{r}^2 + 6 r^2 \dot{\phi}^2 + \tfrac{4 M_{\rm t}}{3r} \right], \tag{31}$$

$$g_\phi^{(\rm gw,pp)} = \tfrac{8 M M'}{5 r^2} \dot{\phi} \left[9\dot{r}^2 - 6 r^2 \dot{\phi}^2 + \tfrac{2 M_{\rm t}}{r} \right]. \tag{32}$$

Note that $\dot{r} \ll r\dot{\phi}$, and consequently, $g_r^{(\rm gw,pp)} \ll g_\phi^{(\rm gw,pp)}$.

Prior to resonance, the tidally induced quadrupole $Q_{\rm ns}^{ij}$ oscillates in phase with the orbit and accelerates the GW radiation (Lai et al. 1994a; Flanagan & Hinderer 2008; see also Appendix C for detailed derivations). In particular, two additional terms need to be included in $g_\phi^{(\rm gw)}$. The first is due to $Q_{\rm ns}^{\langle ij \rangle}$, leading to

$$g_\phi^{(\rm gw,ns)} \simeq -\frac{128}{5}\sqrt{\frac{2\pi}{15}} M R^2 r \Omega^5 \times \sum_{m=\pm 2} \left(\sum_{a,\omega_a>0}^{m_a=m} I_a {\rm Re}\left[C_a\right] + \frac{1}{2} \sum_{ab,\omega_a>0}^{m_a+m_b=-m} J_{ab2m} {\rm Re}\left[C_a C_b\right] \right). \tag{33}$$

Meanwhile, the tidal back-reaction modifies the relation between r and $\dot{\phi} \equiv \Omega$ [see later in equation (39)], causing a correction

$$g_\phi^{(\rm gw,br)} \simeq -\frac{96}{5} M M' \left(\frac{R}{r}\right)^2 \Omega^3 \times \sum_a^{\omega_a>0} \left[W_{l_a m_a} I_a {\rm Re}[C_a] + \left(\frac{1}{2} \sum_{b,lm}^{m_a+m_b=-m} W_{lm} J_{ablm} {\rm Re}[C_a C_b] \right) \right]. \tag{34}$$

Note that its sum with the PP part leads to the intuitive result

$$g_\phi^{(\rm gw,pp)} + g_\phi^{(\rm gw,br)} = -\frac{32}{5} \mu r^3 \Omega^5. \tag{35}$$

Similarly, the Burke–Throne dissipation would also act on the mode. This modifies the dynamics of the mode as [cf. equation (2)]

$$\dot{c}_a + i\omega_a c_a = i\omega_a \left[Z_a + (\text{conservative terms}) \right], \tag{36}$$

where

$$Z_a \simeq i \frac{2}{15} W_{22} \frac{M'}{M_{\rm t}} \left(\frac{R}{r}\right)^3 (m_a r \Omega)^5 \left(I_a + \sum_b^{m_b=0} J_{ab2-m_a} c_b^* \right) e^{-i m_a \phi}, \tag{37}$$

for the $l_a = |m_a| = 2$ modes. The effect of Z_a can be ignored for other modes at the order we are interested in. Note that Z_a leads to an imaginary part to C_a, which then becomes a torque on the orbit

[equation (29)] and contributes to the orbital decay. See Appendix C for more discussions.

We have now outlined all the components in the differential equations we solve numerically. As a brief summary, the quantities we integrate are $(r, \dot{r}, \phi, \dot{\phi}{=}\Omega, C_a)$ and they are governed by equations (25) and (26) for the orbital part and equations (2) and (37) for the eigenmodes. We start the numerical integration at $f_{\rm gw} = \Omega/\pi = 50\,{\rm Hz}$ with $\phi = 0$. We set the initial values of r using the PP Keplerian orbit and $\dot{r}$ by the PP GW decay. The modes are initialized with their linear solution $B_a^{(0)}$ (Section 2.1). Note that this choice of initial condition does not affect the results at $f_{\rm gw} \gtrsim 500\,{\rm Hz}$ where the tidal effects are significant. This is because all the tidal effects have a sharp power-law dependence on $f_{\rm gw}$, which we will see explicitly in Section 4. We terminate our integration at $r/R \simeq 2.3$, corresponding to $r/2 \simeq R + \xi^r(R)$ with $\xi^r(R)$ the radial component of the perturbed fluid evaluated at the surface of the NS and on the equator. In other words, our integration terminates approximately when the two NSs come into contact. In comparison, the innermost stable circular orbit is located at a smaller separation of $r = 6(M + M^{'}) \simeq 1.9R$.

Our main numerical result is shown in Fig. 1 where we compare the tidal phase shift of the time-domain GW waveform with (grey curve) and without (olive curve) the non-linear tide. We derive in the next section the equilibrium configuration of the system, which will allow us analytically understand Fig. 1.

4 EQUILIBRIUM CONFIGURATION

The equilibrium configuration of the system can be obtained by assuming that the GW decay is a slow process. Consequently, terms caused by the GW decay can be dropped from the equation of motion. Our goal is to derive r, E, and $\dot{E}$ in terms of mode amplitude C_a and GW frequency (or equivalently, Ω). Since we derived the analytical solutions to the mode amplitudes in Section 2.2, we have a complete description of the orbit with algebraic expressions only.

First, the tidal interaction modifies the Keplerian orbit. We can derive the relation between r and Ω from equation (25). Ignoring the GW decay and thus the $\ddot{r}$ term, we arrive at

$$r^3 = \frac{M_{\rm t}}{\Omega^2} - \frac{r^2 g_r^{\rm (tide)}}{\Omega^2}, \tag{38}$$

as the modified Kepler's law. We can write $r = r_0 + \Delta r$ with $r_0^3 = M_{\rm t}/\Omega^2$, leading to

$$\frac{\Delta r}{r} \simeq -\frac{1}{3}\frac{r^2 g_r^{\rm (tide)}}{M_{\rm t}} = \frac{2}{3}\sum_{lm}(l+1)W_{lm}\left(\frac{R}{r}\right)^l \times \left(\sum_{a,\omega_a>0}^{m_a=m} I_a {\rm Re}[C_a] + \frac{1}{2}\sum_{ab,\omega_a>0}^{m_a+m_b=-m} J_{ablm}{\rm Re}[C_a C_b]\right). \tag{39}$$

The linear correction is obtained by evaluating the right-hand side of equation (39) in terms of r_0 and including the linear tide only in C_a.

$$\frac{\Delta r^{\rm (lin)}}{r} = \frac{2}{3}\frac{M'}{M}\sum_a^{\omega_a>0}(l+1)W_{lm}^2 I_a^2 R^{2l+1} M_{\rm t}^{-(2l+1)/3} \times \frac{\omega_a \Omega^{(4l+2)/3}}{\omega_a - m_a\Omega}. \tag{40}$$

For $l = l_a = 2$ and in the adiabatic limit ($\Omega \ll \omega_a$), this further simplifies to (Lai et al. 1993, 1994a, b; Flanagan & Hinderer 2008; Hinderer et al. 2010)

$$\frac{\Delta r^{\rm (lin)}}{r} \simeq 2k_2\frac{M'}{M}M_{\rm t}^{-5/3}R^5\Omega^{10/3}, \tag{41}$$

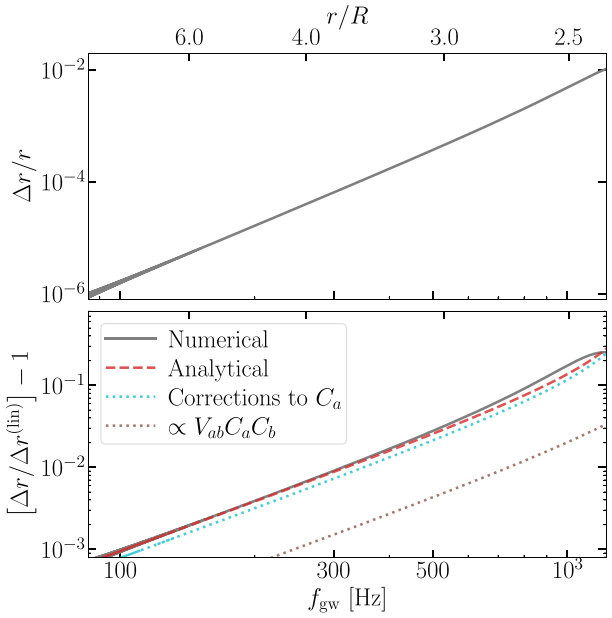

Figure 4. Top: tidal modification of the PP Keplerian orbit, $\Delta r/r$, as a function of GW frequency. Bottom: fractional corrections to the linear theory's prediction on Δr due to non-linear tide. The cyan–dotted curve shows the contribution due to non-linear corrections to the mode amplitude C_a and the brown–dotted curve shows the corrections due to the $V_{ab}C_aC_b$ term.

where we have used equation (6) for Love number k_2.

We can also compute the epicyclic frequency K of the system (Choudhuri 2010) under the linear, adiabatic limit, which reads,

$$K^2 = 4\Omega^2 + r\frac{d\Omega^2}{dr} = \Omega^2\left[1 - 54k_2\frac{M'}{M}\left(\frac{R}{r}\right)^6\right]. \tag{42}$$

For $M^{'} \simeq M$ and $r \simeq 2R$, we have $K^2 \simeq 0.8\Omega^2 > 0$. Including the dynamical response and the non-linear tide will modify K^2 by order unity and we still have $K^2 > 0$. In other words, we do not expect to see a tidally induced plunge throughout the inspiral and the quasi-circular approximation holds.

To compute the next-order corrections, we note that the first non-linear correction to C_a and the non-linear tide piece in $g_r^{\rm (tide)}$ ($\propto {\rm Re}[V_{ab}V_aV_b]$) will both give corrections to $\Delta r/r$ at the order $(R/r)^3[\Delta r^{\rm (lin)}/r] \propto (R/r)^8$. In comparison, errors due to linearization of equation (39) and evaluating its right-hand side at r_0 instead of $r_0 + \Delta r^{\rm (lin)}$ are both on the order $\mathcal{O}\left[\Delta r^{\rm (lin)}/r\right]^2 \propto (R/r)^{10}$. Therefore, we can obtain the leading-order non-linear correction by including the non-linear tide pieces in C_a and $g_r^{\rm (tide)}$ while dropping terms $\propto[\Delta r^{\rm (lin)}/r]^2$. This provides us with an analytical approximation accurate to $(R/r)^8$.

The result of the modification to the Keplerian $r - \Omega$ relation is shown in Fig. 4. In the top panel, we show the total correction to $\Delta r/r$ including both linear and non-linear tides. The fractional correction to the linear theory's prediction due to the non-linear tide is presented in the bottom panel. The grey curve is extracted from the numerical solution to the differential equations described in Sections 2 and 3. The analytical approximation (the red–dashed curve), obtained by substituting the non-linear solution of C_a given by equations (16)–(21) to equation (39) and keeping the $V_{\rm ab}$ terms, agrees well with the numerical result. At $f_{\rm gw} \gtrsim 1000\,{\rm Hz}$ or $(r/R) \lesssim 2.5$, the non-linear tide modifies the linear result by more than 10%. The main effect is

due to the non-linear corrections to the mode amplitudes C_a,[3] which is greater than the contribution from the V_{ab} term by about a factor of 5.

To compute the total energy of the system $\Delta E_{\rm eq} = \Delta E_{\rm orb} + E_{\rm int} + E_{\rm mode}$, we also need to include the energy due to mode–orbit interaction [$E_{\rm int} = H_{\rm int}$; see equation (27)] and the energy of modes

$$\frac{E_{\rm mode}}{E_0} = \sum_a^{\omega_a>0} |c_a|^2 - \frac{1}{3}\sum_{abc}^{\omega_a>0} \kappa_{abc}\left(c_a c_b c_c + c_a^* c_b^* c_c^*\right). \tag{43}$$

The modified $r-\Omega$ relation [equation (39)] modifies the energy of the orbit. The kinetic energy of a quasi-circular orbit is given by

$$E_{\rm orb,k} = \frac{1}{2}\mu r^2\dot{\phi}^2, \tag{44}$$

and the potential energy

$$E_{\rm orb,p} = -\frac{MM'}{r}. \tag{45}$$

It is a well-known result that $E_{\rm orb,\,k} = -E_{\rm orb,\,p}/2 = -E_{\rm orb}$. When tide is present, however, we have

$$\frac{\Delta E_{\rm orb,k}}{E_{\rm orb,k}} = -\frac{\Delta E_{\rm orb,k}}{E_{\rm orb}} = 2\frac{\Delta r}{r}, \tag{46}$$

$$\frac{\Delta E_{\rm orb,p}}{E_{\rm orb,p}} = 2\frac{\Delta E_{\rm orb,p}}{E_{\rm orb}} = -\frac{\Delta r}{r}. \tag{47}$$

Consequently,

$$\frac{\Delta E_{\rm orb}}{E_{\rm orb}} = \frac{\Delta E_{\rm orb,k} + \Delta E_{\rm orb,p}}{E_{\rm orb}} = -4\frac{\Delta r}{r}. \tag{48}$$

For $l = 2$, we also have

$$\frac{E_{\rm int}}{E_{\rm orb}} = 2\frac{\Delta r}{r} = -\frac{1}{2}\frac{\Delta E_{\rm orb}}{E_{\rm orb}}, \tag{49}$$

allowing us to easily obtain the interaction energy.

At the linear order, we get

$$\begin{aligned}\frac{\Delta E_{\rm eq}}{E_{\rm orb}} &= -2\frac{r}{R}\frac{M}{M'}\sum_a^{\omega_a>0}\left[2{\rm Re}\left(V_a C_a^*\right) + |C_a|^2\right], \\ &= -2\frac{M'}{M}M_{\rm t}^{-5/3}R^5\Omega^{10/3} \\ &\times \sum_a^{\omega_a>0} W_{lm}^2 I_a^2\left[2\left(\frac{\omega_a}{\omega_a - m_a\Omega}\right) + \left(\frac{\omega_a}{\omega_a - m_a\Omega}\right)^2\right]\end{aligned} \tag{50}$$

In the adiabatic limit, this further reduces to

$$\frac{\Delta E_{\rm eq}}{E_{\rm orb}} = -6k_2\frac{M'}{M}M_{\rm t}^{-5/3}R^5\Omega^{10/3}. \tag{51}$$

As explained before, to obtain the next order corrections, we include the non-linear tide but drop $(\Delta E_{\rm eq}/E_{\rm orb})^2 \sim (\Delta r/r)^2$ terms. Since we have shown the accuracy of our analytical results in Figs 2 and 4, we show in Fig. 5 the change of the equilibrium energy using the analytical results only. Similar to Fig. 4, we show in the top panel of Fig. 5 the total correction to the equilibrium energy of the system including both linear and non-linear tides, and in the bottom panel the fractional correction to the linear theory's prediction. We again note a $> 10\%$ modification to the linear tide at $f_{\rm gw} \gtrsim 1000\,{\rm Hz}$ and it is mostly due to the non-linear correction to mode amplitudes.

[3]Please note that in this section, the subscript a stands for a mode in general and does not correspond to the specific $l = m = 2$ mode we discussed in Section 2.2.

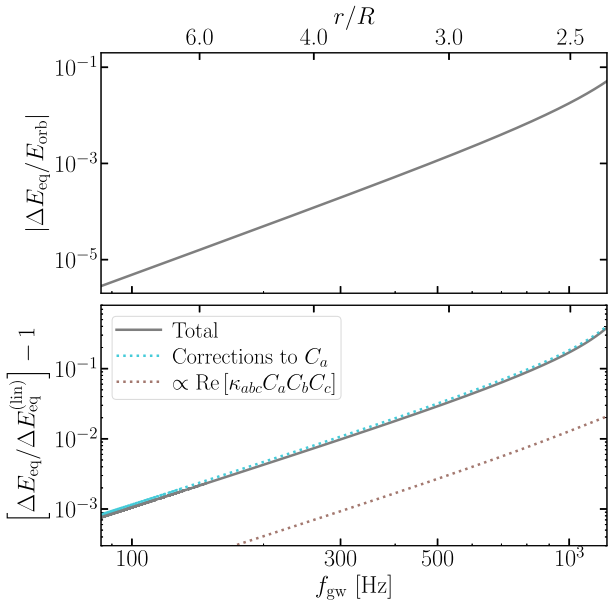

Figure 5. Similar to Fig. 4 but for tidally induced changes in the equilibrium energy, $\Delta E_{\rm eq}$. In the bottom panel, we see that the dominant non-linear effect comes from the corrections to the mode amplitude C_a while the energy in the non-linear interaction ($\propto {\rm Re}[\kappa_{\rm abc}C_aC_bC_c]$) is subdominant.

The last piece we need is the energy flux $\dot{E} = -\langle \dddot{Q}_{\rm tot}^{\langle ij\rangle}\dddot{Q}_{\rm tot}^{\langle ij\rangle}\rangle/5$ (see, e.g. Poisson & Will 2014). It is enhanced by the tidal interaction due to two main effects. The first one comes from the coupling between the tidal and orbital quadrupoles, which can be written as

$$\Delta\dot{E}_{\rm ns-orb} = -\frac{2}{5}\left\langle \dddot{Q}_{\rm ns}^{\langle ij\rangle}\dddot{Q}_{\rm orb}^{\langle ij\rangle}\right\rangle. \tag{52}$$

This piece has the same origin as the dissipative accelerations due to $g_\phi^{\rm (gw,ns)}$ and Z_a in the differential equations (Section 3). Using techniques described in Appendix C, we find

$$\Delta\dot{E}_{\rm ns-orb} = -\frac{4}{15}\sum_m W_{2m}\left\langle \dddot{Q}_{2m}^{\rm ns}\ddot{Q}_{2m}^{\rm orb*}\right\rangle, \tag{53}$$

where $Q_{2m}^{\rm ns}$ and $Q_{2m}^{\rm orb}$ are, respectively, the mass quadrupole of the NS and the orbit with spherical degree $(2, m)$ (see Appendix C).

When the GW decay is slow, we have

$$\begin{aligned}\dddot{Q}_{2m}^{\rm ns} &\simeq (-im\Omega)^3 Q_{2m}^{\rm ns} \\ &= (-im\Omega)^3 MR^2\left[\sum_a^{m_a=m} I_a C_a + \frac{1}{2}\sum_{ab}^{m_a+m_b=-m} J_{ab2m}C_a^*C_b^*\right]e^{-im\phi},\end{aligned} \tag{54}$$

and

$$\ddot{Q}_{2m}^{\rm orb*} \simeq (im\Omega)^3 Q_{2m}^{\rm orb*} = (im\Omega)^3\mu r^2 e^{im\phi}. \tag{55}$$

Thus ,

$$\begin{aligned}\Delta\dot{E}_{\rm ns-orb} &= -\frac{8}{15}\mu MR^2 M_{\rm t}^{2/3}\Omega^{14/3}\sum_{m=\pm2} m^6 W_{2m} \\ &\times\left(\sum_{a,\omega_a>0}^{m_a=m} I_a{\rm Re}\left[C_a\right] + \frac{1}{2}\sum_{ab,\omega_a>0}^{m_a+m_b=-m} J_{ab2m}{\rm Re}\left[C_aC_b\right]\right).\end{aligned} \tag{56}$$

Note the summation runs over positive-frequency modes for a while it runs over both signs of frequency for mode b in the non-linear term.

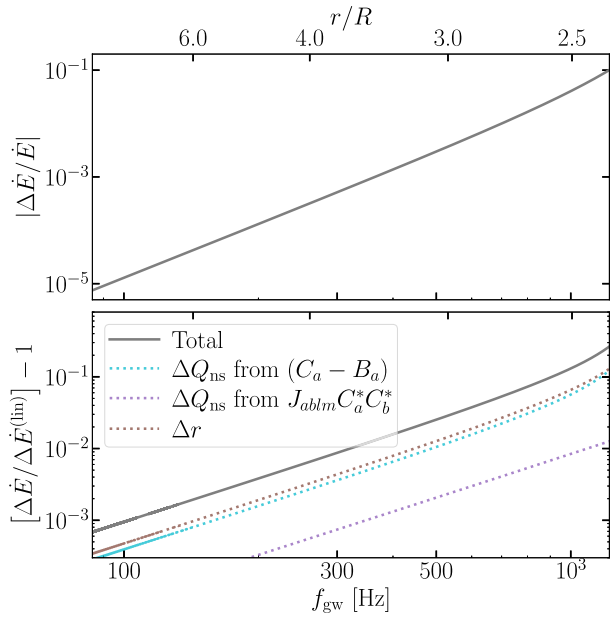

Figure 6. Similar to Fig. 4 but for the energy flux $\dot{E}$. In the bottom panel, we show non-linear corrections to the energy flux from both the modifications of the NS quadrupole (cyan and purple curves) and the non-linear $r-\Omega$ relation (Fig. 4).

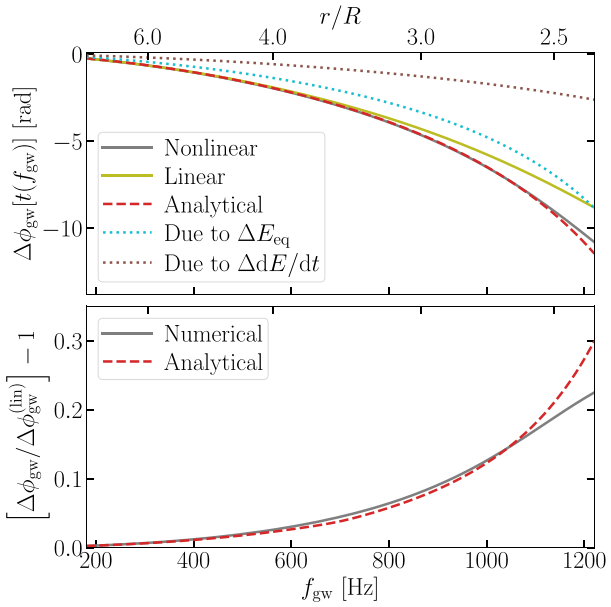

Figure 7. GW phase shift as a function of GW frequency (bottom axis) and orbital separation (top axis). The top panel is similar to Fig. (1). We further include the analytical approximation from equation (61) in the red–dashed curve and it agrees well with the numerical result in the grey curve. The contribution to the phase shift from the modified equilibrium energy and the enhanced GW radiation are shown in the cyan–dotted and brown–dotted lines. In the bottom panel, we show the fraction correction to the phase shift predicted by linear tide. The correction is greater than 10% at $f_{\rm gw} \gtrsim 1000$ Hz.

In the linear, adiabatic limit, the result reduces to (Lai et al. 1994a)

$$\frac{\Delta\dot{E}_{\rm ns-orb}}{\dot{E}_{\rm pp}} = 4k_2\frac{M_{\rm t}}{M}R^5 M_{\rm t}^{-5/3}\Omega^{10/3}, \tag{57}$$

where we have used

$$\dot{E}_{\rm pp} = -\frac{32}{5}\mathcal{M}_c^{10/3}\Omega^{10/3}, \tag{58}$$

for the PP GW radiation with $\mathcal{M}_c = \mu^{3/5}M_{\rm t}^{2/5}$ the chirp mass.

The second effect that enhances $\dot{E}$ is the tide-modified $r-\Omega$ relation, which enhances the $\left\langle \dddot{Q}_{\rm orb}^{\langle ij\rangle}\dddot{Q}_{\rm orb}^{\langle ij\rangle}\right\rangle$ term compared to the PP case [corresponding to the $g_\phi^{\rm (gw,br)}$ term; equation (34)]. Since $Q_{\rm orb}\sim r^2$, the correction to the energy flux is due to modified $r-\Omega$ relation given by

$$\frac{\Delta\dot{E}_{r-\Omega}}{\dot{E}_{\rm pp}} = 4\frac{\Delta r}{r}. \tag{59}$$

The total enhancement of the energy loss is thus given by $\Delta\dot{E} = \Delta\dot{E}_{\rm ns-orb} + \Delta\dot{E}_{r-\Omega}$. This ignores the contribution from $\langle\dddot{Q}_{\rm ns}^{\langle ij\rangle}\dddot{Q}_{\rm ns}^{\langle ij\rangle}\rangle$, which is a higher-order correction than the non-linear tide we consider in this study [see the discussion around equation (C33)].

We present in Fig. 6 the results of $\Delta\dot{E}$. We note similar non-linear corrections to $\Delta\dot{E}$ (lower panel) from the interaction between NS and orbital quadrupoles [equation (56)] and from the modification to the $r-\Omega$ relation [equation (59)]. In both effects, the non-linear correction comes mainly from its correction to the mode amplitudes $(C_a - B_a)$ whereas the $\propto J_{\boldsymbol{ablm}}$ term is subdominant.

From $E_{\rm eq}$ and $\dot{E}$, we can get the phase of the GW signal as (Lai et al. 1994b; Hinderer et al. 2010)

$$\frac{{\rm d}\phi_{\rm gw}}{{\rm d}f_{\rm gw}} = 2\pi f_{\rm gw}\frac{{\rm d}E/{\rm d}f_{\rm gw}}{\dot{E}}. \tag{60}$$

Note that $\phi_{\rm gw} = 2\phi$ is the phase of the time-domain waveform expressed as a function of $f_{\rm gw}$. The phase shift due to the tidal effect is

$$\frac{{\rm d}\Delta\phi_{\rm gw}}{{\rm d}f_{\rm gw}} = \frac{2\pi f_{\rm gw}}{\dot{E}}\left(\frac{{\rm d}\Delta E_{\rm eq}}{{\rm d}f_{\rm gw}} - \frac{{\rm d}E_{\rm eq}}{{\rm d}f_{\rm gw}}\frac{\Delta\dot{E}}{\dot{E}}\right). \tag{61}$$

As noted in the discussion below equation (41), the corrections due to the second-order expansion [i.e. terms like $(\Delta E_{\rm eq}/E_{\rm eq})^2$] are smaller than the non-linear tide we consider by a factor of $(R/r)^2$ and are thus ignored in the expression.

Our final result is presented in Fig. 7 (also in Fig. 1). In the top panel, we show the total phase shift due to tidal effects in the NS M (while treating M' as a PP). The olive curve is the prediction assuming just the linear tide while the grey curve also includes the non-linear tide. Both curves are obtained by numerically solving the differential equations described in Sections 2 and 3. For comparison, the red–dashed curve shows the analytical phase shift [equation (61)]. We note a good agreement between the analytical and numerical results. The effects due to the modified equilibrium energy and the modified GW radiation are, respectively, shown in the cyan–dotted and brown–dotted curves. The fractional correction to the linear tidal phase shift is shown in the bottom panel.

For a Newtonian NS, non-linear tide could introduce an additional 2 rad of phase shift, corresponding to about 20 per cent enhancement of the tidal effect near the final merger. GR is likely to reduce the result because the NS will be 'softer' (harder to perturb). As we argue in Section 5, after the GR correction, the excess phase shift due to non-linear tide should be around 1 rad. This is consistent with the discrepancy between the state-of-art theoretical models assuming linear tides in GR and numerical relativity (Hinderer et al. 2016; Steinhoff et al. 2021). Therefore, our result suggests that including non-linear tidal interactions could explain the discrepancy and allow the theoretical models to be accurate all the way to the final merger.

5 CONCLUSION AND DISCUSSIONS

In this work, we investigated tidal interactions in coalescing BNS including leading-order non-linear corrections. We discussed the dynamics of the NS eigenmodes and the orbit in Sections 2 and 3, respectively. Utilizing analytical approximations to the mode amplitudes in Section 2.2, we derived algebraic solutions governing the binary's evolution track and the corresponding GW phase in Section 4. For a Newtonian NS approximated by a $\Gamma = 2$ polytrope, we found that the non-linear tide could lead to an additional ~ 2 rad phase shift in the GW waveform near the binary's final merger. While this is likely an overestimation of the non-linear effect because a Newtonian NS is stiffer than its GR counterpart, our result suggests that the non-linear tide is a critical component to be included in the waveform modelling and it could improve the agreement between theoretical models and numerical relativity, especially near the final merger.

Incorporating GR corrections is thus one of the major future steps to obtain a robust theoretical estimate of the non-linear tide. In particular, there are two major GR effects to be considered and they act in opposite directions. First, we note that the relativistic value of the Love number, $k_2 \propto I_a^2$, is smaller than its Newtonian counterpart by a factor of 2–3 (Binnington & Poisson 2009; Damour & Nagar 2009; Hinderer et al. 2010), reducing the linear tidal phase shift accordingly. The phase shift induced by non-linear tidal corrections may scale as k_2^2 because the non-linear correction to the mode amplitude is sourced by the square of the linear amplitude (assuming that GR has similar effects on the linear tidal overlaps and the non-linear coupling coefficients). This could reduce the non-linear correction to the phase by a factor of $\sim 5-10$.

While GR reduces the spatial coupling, it nonetheless enhances the finite-frequency effect by lowering the mode frequency ω_a. When perturbing the *same* background model, the GR oscillation equations typically result in smaller eigenfrequencies than the Newtonian result (Yu & Weinberg 2017b) due to the redshift of the NS itself $\propto M/R$. Moreover, the orbit will further redshift ω_a to a lower value by a factor $\propto M_t/r$ ($\sim 20\%$ near the merger; see, e.g. Steinhoff et al. 2016, 2021). For $|m| = 2$ modes, lowering ω_a enhances the finite-frequency response via of $\omega_a/(\omega_a + \Delta\omega_a - m_a\Omega)$ [equation (20)], while for $m = 0$, ΔV_c will be greater [equation (19)]. The non-linear corrections to $\Delta r/r$ (and similarly to $\Delta E_{\rm eq}/E_{\rm eq}$ and $\Delta\dot{E}/\dot{E}$) go approximately as $\omega_a^2/(\omega_a^2 - 4\Omega^2)$. Reducing ω_a by 35% will amplify $\omega_a^2/(\omega_a^2 - 4\Omega^2)$ by about a factor of 2 when $f_{\rm gw} = \Omega/\pi = 1000$ Hz. This partially compensates for the reduction of the phase shift due to the reduced coupling strength. After considering both GR effects, our estimation of the non-linear tide's contribution to the phase shift becomes $|\Delta\phi_{\rm gw}| \simeq 1$ rad (including contributions from both NSs) near the merger.

Exploring the non-linear contribution to a wide range of EoSs will be another important extension. The non-linear tide is likely to exhibit a stronger dependence on the EoS than the linear tide because it is sourced by the square of the linear tidal amplitude. It could therefore strengthen the constraints on the NS EoS potentially, though this remains to be shown by future studies. Along the same line, it would be interesting to examine if a universal relation exists between the non-linear coupling strength and other properties of the NS (in analogy to the universal relation between the Love number and NS mass quadrupole; Yagi & Yunes 2013).

We assumed a non-spinning NS in our analysis. If the NS has a retrograde spin relative to the orbit, the f-mode could be shifted to a lower frequency due to both the Doppler effect and modifications to the NS structure. If the spin rate is sufficiently high, the $l_a = m_a = 2$ f-mode could even be resonantly excited (Ho & Lai 1999; Ma et al. 2020; Steinhoff et al. 2021). Alternatively, the f-mode could be resonantly excited if the orbit has some residual eccentricity when the binary enters the sensitivity band of a ground-based GW detector (Chirenti et al. 2017; Parisi & Sturani 2018; Yang et al. 2018; Vick & Lai 2019; Yang 2019; Wang & Lai 2020). Since the non-linear correction is amplified by the finite-frequency response of the NS, we may thus expect the non-linear tide to play an even more significant role in those systems. The standard anharmonic frequency shift could also be significant since $m = 2$ f-mode can have much greater amplitude than other $l = 2$ modes (see Appendix B). In turn, as the non-linear frequency shift lowers the mode frequency, it makes the resonance more likely, which enhances the overall tidal signatures. Thus incorporating NS spin and orbital eccentricities are also potentially interesting extensions to the current study.

Another simplification assumed in this work is that we modelled the fluid inside the NS as a normal fluid. In reality, we would expect the NS to be cold and its core is likely in the superfluid state (Yakovlev, Levenfish & Shibanov 1999). Passamonti et al. (2022) showed that the correction due to superfluidity is small for f-modes, and we thus expect our main results to hold in realistic NSs. Nonetheless, a careful calculation incorporating superfluidity would be worthwhile.

ACKNOWLEDGEMENTS

HY's work at KITP is supported by the National Science Foundation (NSF PHY-1748958) and by the Simons Foundation (216179, LB). NNW and PA acknowledge support from NSF AST-2054353. JK and TV acknowledge support from NSF PHY-2012086.

DATA AVAILABILITY

The main data underlying this article are available in the article. Additional information may be requested from the authors.

REFERENCES

Abbott B. P. et al., 2017, Class. Quantum Gravity, 34, 044001
Alford M. G., Haber A., Harris S. P., Zhang Z., 2021, Universe, 7, 399
Andersson N., Ho W. C. G., 2018, Phys. Rev. D, 97, 023016
Andersson N., Pnigouras P., 2020, Phys. Rev. D, 101, 083001
Andersson N., Pnigouras P., 2021, MNRAS, 503, 533
Arras P., Weinberg N. N., 2019, MNRAS, 486, 1424
Bernuzzi S., Nagar A., Dietrich T., Damour T., 2015, Phys. Rev. Lett., 114, 161103
Bini D., Damour T., 2014, Phys. Rev. D, 90, 124037
Binnington T., Poisson E., 2009, Phys. Rev. D, 80, 084018
Chirenti C., Gold R., Miller M. C., 2017, ApJ, 837, 67
Choudhuri A. R., 2010, Astrophysics for Physicists. Cambridge University Press, New York
Cowling T. G., 1941, MNRAS, 101, 367
Damour T., Nagar A., 2009, Phys. Rev. D, 80, 084035
Damour T., Nagar A., Villain L., 2012, Phys. Rev. D, 85, 123007
Del Pozzo W., Li T. G. F., Agathos M., Van Den Broeck C., Vitale S., 2013, Phys. Rev. Lett., 111, 071101
Essick R., Vitale S., Weinberg N. N., 2016, Phys. Rev. D, 94, 103012
Evans M. et al., 2021, preprint (arXiv:2109.09882)
Flanagan É. É., Hinderer T., 2008, Phys. Rev. D, 77, 021502
Flanagan É. É., Racine É., 2007, Phys. Rev. D, 75, 044001
Foucart F. et al., 2019, Phys. Rev. D, 99, 044008
Gupta P. K., Steinhoff J., Hinderer T., 2021, Phys. Rev. Res., 3, 013147
Hild S., Chelkowski S., Freise A., Franc J., Morgado N., Flaminio R., DeSalvo R., 2010, Class. Quantum Gravity, 27, 015003

Hinderer T., Lackey B. D., Lang R. N., Read J. S., 2010, Phys. Rev. D, 81, 123016
Hinderer T. et al., 2016, Phys. Rev. Lett., 116, 181101
Ho W. C. G., Lai D., 1999, MNRAS, 308, 153
Hotokezaka K., Kyutoku K., Okawa H., Shibata M., 2015, Phys. Rev. D, 91, 064060
Kuan H.-J., Suvorov A. G., Kokkotas K. D., 2021a, MNRAS, 506, 2985
Kuan H.-J., Suvorov A. G., Kokkotas K. D., 2021b, MNRAS, 508, 1732
Kumar P., Goldreich P., Kerswell R., 1994, ApJ, 427, 483
Lackey B. D., Wade L., 2015, Phys. Rev. D, 91, 043002
Lai D., 1994, MNRAS, 270, 611
Lai D., 1996, Phys. Rev. Lett., 76, 4878
Lai D., Rasio F. A., Shapiro S. L., 1993, ApJS, 88, 205
Lai D., Rasio F. A., Shapiro S. L., 1994a, ApJ, 420, 811
Lai D., Rasio F. A., Shapiro S. L., 1994b, ApJ, 423, 344
Landau L., Lifshitz E., 1982, Mechanics, Vol. 1. No. v. 1. Elsevier Science, Oxford, UK
Landry P., Essick R., 2019, Phys. Rev. D, 99, 084049
LIGO Scientific Collaboration, Virgo Collaboration et al., 2017, Phys. Rev. Lett., 119, 161101
LIGO Scientific Collaboration, Virgo Collaboration et al., 2018, Phys. Rev. Lett., 121, 161101
LIGO Scientific Collaboration, Virgo Collaboration et al., 2019a, Phys. Rev. X, 9, 011001
LIGO Scientific Collaboration, Virgo Collaboration Weinberg N. N. et al., 2019b, Phys. Rev. Lett., 122, 061104
LIGO Scientific Collaboration, Virgo Collaboration et al., 2020, ApJ, 892, L3
Ma S., Yu H., Chen Y., 2020, Phys. Rev. D, 101, 123020
Ma S., Yu H., Chen Y., 2021, Phys. Rev. D, 103, 063020
Matas A. et al., 2020, Phys. Rev. D, 102, 043023
Messenger C., Read J., 2012, Phys. Rev. Lett., 108, 091101
Nagar A. et al., 2018, Phys. Rev. D, 98, 104052
Pan Z., Lyu Z., Bonga B., Ortiz N., Yang H., 2020, Phys. Rev. Lett., 125, 201102
Parisi A., Sturani R., 2018, Phys. Rev. D, 97, 043015
Passamonti A., Andersson N., Pnigouras P., 2021, MNRAS, 504, 1273
Passamonti A., Andersson N., Pnigouras P., 2022, MNRAS, 514, 1494
Poisson E., 2020, Phys. Rev. D, 101, 104028
Poisson E., Will C. M., 2014, Gravity. Cambridge University Press, Cambridge, UK
Pratten G., Schmidt P., Williams N., 2022, Phys. Rev. Lett., 129, 081102
Read J. S., Markakis C., Shibata M., Uryū K., Creighton J. D. E., Friedman J. L., 2009, Phys. Rev. D, 79, 124033
Reisenegger A., Goldreich P., 1994, ApJ, 426, 688
Saffer A., Yagi K., 2021, Phys. Rev. D, 104, 124052
Sathyaprakash B. et al., 2012, Class. Quantum Gravity, 29, 124013
Schenk A. K., Arras P., Flanagan É. É., Teukolsky S. A., Wasserman I., 2002, Phys. Rev. D, 65, 024001
Steinhoff J., Hinderer T., Buonanno A., Taracchini A., 2016, Phys. Rev. D, 94, 104028
Steinhoff J., Hinderer T., Dietrich T., Foucart F., 2021, Phys. Rev. Res., 3, 033129
Thorne K. S., 1980, Rev. Mod. Phys., 52, 299
Townsend R. H. D., Teitler S. A., 2013, MNRAS, 435, 3406
Townsend R. H. D., Goldstein J., Zweibel E. G., 2018, MNRAS, 475, 879
Tsang D., Read J. S., Hinderer T., Piro A. L., Bondarescu R., 2012, Phys. Rev. Lett., 108, 011102
Van Hoolst T., 1994, A&A, 286, 879
Venumadhav T., Zimmerman A., Hirata C. M., 2014, ApJ, 781, 23
Vick M., Lai D., 2019, Phys. Rev. D, 100, 063001
Wang J.-S., Lai D., 2020, Phys. Rev. D, 102, 083005
Weinberg N. N., 2016, ApJ, 819, 109
Weinberg N. N., Arras P., Quataert E., Burkart J., 2012, ApJ, 751, 136
Weinberg N. N., Arras P., Burkart J., 2013, ApJ, 769, 121
Wu Y., 1998, PhD thesis. California Institute of Technology, https://thesis.library.caltech.edu/3736/
Xu W., Lai D., 2017, Phys. Rev. D, 96, 083005
Yagi K., Yunes N., 2013, Science, 341, 365
Yakovlev D. G., Levenfish K. P., Shibanov Y. A., 1999, Phys. Usp., 42, 737
Yang H., 2019, Phys. Rev. D, 100, 064023
Yang H., East W. E., Paschalidis V., Pretorius F., Mendes R. F. P., 2018, Phys. Rev. D, 98, 044007
Yu H., Weinberg N. N., 2017a, MNRAS, 464, 2622
Yu H., Weinberg N. N., 2017b, MNRAS, 470, 350
Yu H., Weinberg N. N., Fuller J., 2020, MNRAS, 496, 5482
Yu H., Weinberg N. N., Arras P., 2021, ApJ, 917, 31
Yu H., Weinberg N. N., Arras P., 2022, ApJ, 928, 140

APPENDIX A: A TOY MODEL DEMONSTRATING THE F-MODE FREQUENCY SHIFTS

The frequency shift of the f-modes derived in equation (16) can be understood from a toy model illustrated in the left part of Fig. A1. Imagine we drill a hole through the centre of a uniform-density star in the equatorial plane where the $l = 2$, $|m| = 2$ f-modes mainly reside. If we drop a test particle into the hole (red dot in Fig. A1), the particle will oscillate inside the hole as a harmonic oscillator. When the particle is at x, it feels an inward acceleration $g = 4\pi\rho x/3$, and its equation of motion is given by $\ddot{x} = -4\pi\rho x/3 = -\omega^2 x$. The oscillation frequency is

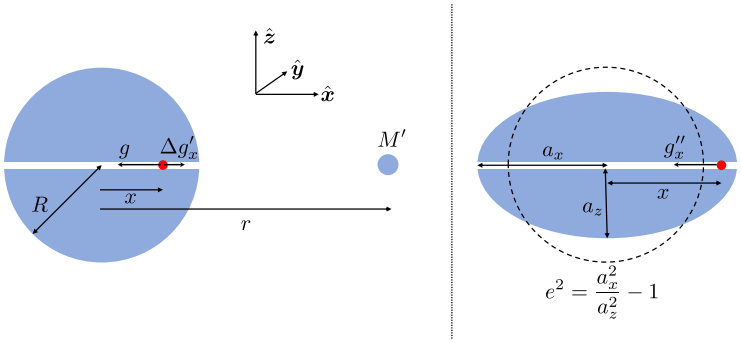

Figure A1. A toy model demonstrating the origin of the f-mode frequency shift. A test particle released in a hole through a star's centre will oscillate in the hole as a harmonic oscillator with the same frequency as the f-mode (up to an order unity constant). On the left, the oscillation frequency of the test particle is reduced by the tidal acceleration $\Delta g'_x$ from a companion of mass M' [similar to equation (16)]. On the right, the oscillation frequency is reduced by the tidal deformation of the background star caused by the f-modes, corresponding to the oscillator's anharmonicity (Appendix B).

therefore $\omega = \sqrt{4\pi\rho/3}$, the same as the f-mode frequency up to an order unity constant. Indeed, both oscillations are similar in nature as they are both characterized by the dynamical frequency of the star.

If now a companion of mass M' is present in the equatorial plane and the separation vector is along the direction of the hole (in the x direction), then M' will produce a tidal acceleration $\Delta g'_x = 2\left(M'/r^2\right)(x/r)$ in the opposite direction of g. In this case, the test particle still behaves as a harmonic oscillator, though its equation of motion is now modified by $\Delta g'_x$ as

$$\ddot{x} = -(g - \Delta g'_x) = -\frac{4\pi}{3}\rho\left[1 - 2\left(\frac{M'}{M}\right)\left(\frac{R}{r}\right)^3\right]x = -\omega^2\left(1 + 2\frac{\Delta\omega_x}{\omega}\right)x. \tag{A1}$$

If instead, the hole is perpendicular to the orbital vector but still in the equatorial plane (i.e. along the y direction), then a test particle oscillating in it experiences a tidal acceleration $|\Delta g'_y| = \left(M'/r^2\right)(y/r)$ pointing towards the centre of the star. In this case, the oscillation is increased by $\Delta\omega_y/\omega_y = (M'/M)(R/r)^3/2 = -\Delta\omega_x/\omega/2$ due to M'. Since the $l = 2$, $|m| = 2$ f-modes mainly oscillate in the equatorial plane, it experiences a frequency shift that is approximately the mean of these two results,

$$\frac{\Delta\omega}{\omega} \sim \frac{1}{2}\frac{\Delta\omega_x + \Delta\omega_y}{\omega} = -\frac{1}{4}\frac{M'}{M}\left(\frac{R}{r}\right)^3 = -\frac{1}{4}\frac{M'}{M}\frac{\Omega^2}{M_{\rm t}}R^3 < 0. \tag{A2}$$

Up to a constant of order unity, this agrees with the leading-order frequency shift of the f-mode found in Section 2.2 and given by equation (16). In other words, the presence of the companion's tidal field reduces the eigenfrequency of the f-mode, thereby enhancing the finite frequency response to the tidal drive.

If we further let the star to be deformed by the tide into an ellipsoid (with $a_x > R$ and $a_y = a_z < R$; see the right part of Fig. A1), then the gravitational acceleration g should be replaced by $g''_x = (1 - 2e^2/5)g$ along the x direction, where $e = \sqrt{a_x^2/a_z^2 - 1} \propto \xi^r(R)/R \propto |C_a|$ is the eccentricity of the ellipsoid. The reduction of the inward gravitational acceleration will also cause a frequency shift of the test particle's oscillation (see, e.g. Poisson & Will 2014),

$$\frac{\Delta\omega_x}{\omega} = \frac{1}{2}\frac{g''_x - g}{g} = -\frac{1}{5}e^2 \propto |C_a|^2 \propto \left(\frac{R}{r}\right)^6. \tag{A3}$$

The oscillation frequency along the y direction will increase since the gravitational acceleration along the y direction is $g''_y = (1 + e^2/5)g$. None the less, $\Delta\omega_y = -\Delta\omega_x/2$, and therefore, on average the $l = |m| = 2$ f-modes will experience a negative frequency shift $\Delta\omega/\omega \sim -1/e^2 < 0$. Such a frequency shift can also be understood from the fact that the tidal deformation tends to reduce the density of the star Lai (1996), hence reducing the f-mode frequency $\propto \sqrt{\rho}$. We note that the frequency shift due to this effect is formally a higher-order correction than the shift induced directly by the companion's tidal acceleration in equation (A2). In fact, equation (A3) describes the anharmonicity of an oscillator. A detailed derivation of the anharmonicity from the modal expansion analysis is presented in Appendix B below.

APPENDIX B: ANHARMONIC FREQUENCY SHIFT

We extend the analysis in Section 2.2 to demonstrate the appearance of the anharmonicity in the modal picture. We will also demonstrate the significance of including four-mode coupling terms [terms $\propto\eta_{abcd}$ in equation (2)] in solving the numerical equations.

We use the same convention adopted in Section 2.2 and use (a, b, c) to specifically denote $l = 2$ modes with $(m_a, m_b, m_c) = (2, -2, 0)$. Since only the a mode will experience the most significant dynamical tide effect near the merger when $2\Omega \lesssim \omega_a$, we thus solve C_b and C_c in terms of C_a as well as their linear solutions B_b and B_c. We have

$$C_b \simeq B_b + \frac{\omega}{\omega + 2\Omega}\left(V_{20} + 4\kappa_2{\rm Re}[B_c]\right)C_a^* + \Delta C_b, \tag{B1}$$

$$C_c \simeq B_c + 2\kappa_2|C_a|^2 + 2V_{22}{\rm Re}\left[C_a\right] + 4\kappa_2{\rm Re}\left[C_a B_b\right] + \Delta C_c, \tag{B2}$$

where

$$\Delta C_b \simeq \frac{\omega}{\omega + 2\Omega}\left(V_{20}B_b + 4\kappa_2{\rm Re}\left[B_c\right]B_b + 2V_{22}{\rm Re}\left[B_c\right]\right), \tag{B3}$$

$$\Delta C_c \simeq 2\left(V_{22}{\rm Re}\left[B_b\right] + V_{00}{\rm Re}\left[B_c\right] + \kappa_2|B_b|^2 + \kappa_0{\rm Re}\left[B_c B_c\right] + \kappa_0|B_c|^2\right). \tag{B4}$$

Plugging C_b and C_c back to the equation of C_a, we have

$$\dot{C}_a + i(\omega_a + \Delta\omega_a^{(3{\rm m})} - m_a\dot{\phi})C_a = i\omega_a[V_a + \Delta V_a^{(3{\rm m})}], \tag{B5}$$

where

$$\begin{aligned}\Delta V_a^{(3{\rm m})} = {} & V_{20}B_b^* + 2V_{22}{\rm Re}[B_c] + 4\kappa_2 B_b^*{\rm Re}[B_c] + 4\kappa_2(V_{22} + 2\kappa_2 B_b^*)|C_a|^2 \\ & + 4|V_{22} + 2\kappa_{22}B_b|^2{\rm Re}[C_a] + V_{20}\Delta C_b^* + 2V_{22}{\rm Re}[\Delta C_c] + 4\kappa_2 B_b^*{\rm Re}[\Delta C_c] + 4\kappa_2{\rm Re}[B_c]\Delta B_b^*,\end{aligned} \tag{B6}$$

and

$$\begin{aligned}\left(\frac{\Delta\omega_a}{\omega_a}\right)^{(3{\rm m})} = {} & -(V_{20} + 4\kappa_2{\rm Re}[B_c]) - 8\kappa_2^2|C_a|^2 \\ & - 8\kappa_2 V_{22}{\rm Re}[C_a] - 16\kappa_2^2\left[B_b C_a\right] - \frac{\omega_a}{\omega_a + 2\dot{\phi}}(V_{20} + 4\kappa_2{\rm Re}[B_c])^2 - 4\kappa_2{\rm Re}[\Delta C_c].\end{aligned} \tag{B7}$$

As shown in Fig. 3, our focus will be on the frequency shift. In equation (B7), the first term is the result we quote in equation (16) as it formally scales as $(R/r)^3$ while the rest of the terms $\propto (R/r)^6$. Note that this term exists because the system is continuously forced by the tide and $|V_{20}| \sim |C_c| \sim |C_a|$.

On the other hand, we may have $|C_a| \gg |V_{20}| \sim |C_c|$ if mode a is resonantly excited due to, e.g. a rotating NS (Ma et al. 2020; Steinhoff et al. 2021) and/or orbital eccentricity (Yang 2019). In this limit, the $-8\kappa_2^2|C_a|^2$ term may dominant the frequency shift. Since $|C_a|^2$ corresponds to the energy of mode a, we notice that it corresponds to the anharmonicity of a *free* oscillator (Landau & Lifshitz 1982). As discussed in Yu et al. (2021), mode a can couple to not only $l = 2$ modes but also $l = 0$ and $l = 4$ ones. The total anharmonic frequency shift of mode a due to three-mode interaction can be written as

$$\left(\frac{\Delta\omega_a}{\omega_a}\right)^{(3\mathrm{m})} \simeq -\left(\sum_{d,m_d=-4}^{l_d=4} \frac{2\omega_d}{4\Omega+\omega_d}\kappa_{aad}^2 + \sum_{e,m_e=0}^{l_e=0,2,4} 4\kappa_{aa^*e}^2\right)|C_a|^2. \tag{B8}$$

We have dropped terms that do not scale as $|C_a|^2$ since we have assumed that mode a is approximated by a free oscillator with its amplitude much greater than other modes and the equilibrium tide.

Formally at the same order, four-mode coupling could also contribute to the anharmonic frequency shift.[4] We only explicitly write out the equation for C_a.

$$\begin{aligned}\dot{C}_a + i(\omega_a - m_a\dot{\phi})C_a = &\,(\text{linear and three-mode terms}) + i\omega_a(3\eta_{aaa^*a^*}|C_a|^2C_a \\ &+ 6\eta_{aaa^*b}|C_a|^2C_b^* + 3\eta_{aa^*a^*b^*}C_a^2C_b + 6\eta_{aa^*bb^*}C_a|C_b|^2 + 3\eta_{aabb}C_a^*(C_b^*)^2 \\ &+ 6\eta_{aa^*cc^*}C_a|C_c|^2 + 3\eta_{aa^*cc}C_a(C_c^*)^2 + 3\eta_{aa^*c^*c^*}C_aC_c^2 \\ &+ 3\eta_{abbb^*}|C_b|^2C_b + 6\eta_{abcc^*}C_b|C_c|^2 + 3\eta_{abcc}C_b(C_c^*)^2 + 3\eta_{abc^*c^*}C_bC_c^2).\end{aligned} \tag{B9}$$

By collecting terms $\propto C_a$ on the right-hand side, we can read out directly the four-mode contributions to the anharmonic frequency shift.

$$\left(\frac{\Delta\omega_a}{\omega_a}\right)^{(4\mathrm{m})} \simeq -3\eta_{22}|C_a|^2 - 3\eta_{22}C_aC_b - 6\eta_{22}|C_b|^2 - 12\eta_{20}|C_c|^2 \simeq -3\eta_{22}|C_a|^2, \tag{B10}$$

where we have made the approximation that $C_c \simeq C_c^*$ and defined

$\eta_{22} = \eta_{aaa^*a^*}$ and similar terms,

$\eta_{20} = \eta_{aa^*cc^*}$ and similar terms.

[4] In the original analysis of Yu et al. (2021) (and in Kumar et al. 1994), the four-mode contribution was ignored. Additionally, there was a numerical error that overestimates the contribution of p-modes to the frequency shift. An erratum to Yu et al. (2021) is under preparation at the moment of preparing this work.

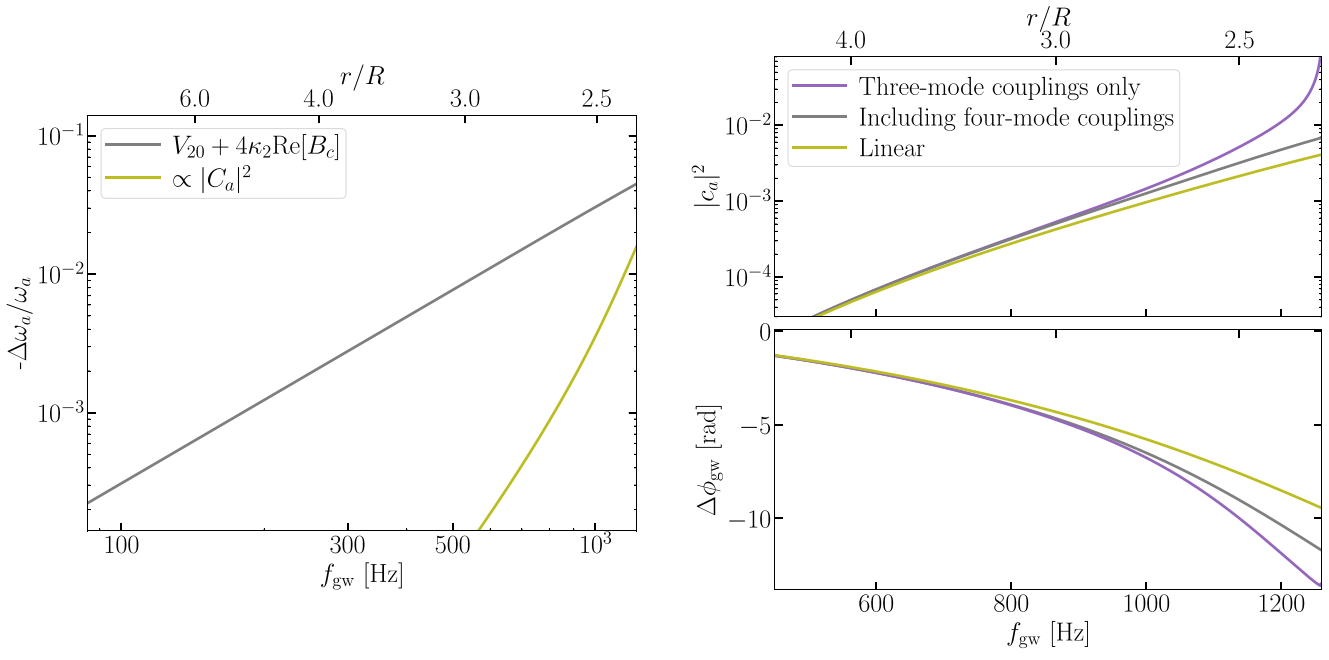

Figure B1. Left: comparison of the non-linear frequency shift. The grey trace is the result from equation (16), which we use in the main text, while the olive curve is due to the anharmonicity [the sum of terms $\propto|C_a|^2$ in equations (B8) and (B10)]. Because the finite-frequency effect is moderate in non-rotating, Newtonian NSs, the anharmonicity is small and can be ignored. Right: comparison of mode energy (of the $l_a = m_a = 2$ mode) and GW phase shift with (grey) and without (purple) four-mode coupling terms. Near the final merger, the three-mode-only result in fact experiences an artificial run away. It thus indicates the significance of incorporating four-mode couplings in the numerical integration.

Their values are in Table 1. In the second equality in equation (B10), we dropped terms that do not scale as $|C_a|^2$ since the anharmonic effect could be significant only if $|C_a| \gg |C_{b,c}|$. This is also why we ignore the four-mode counterpart of the U_{ablm} term as it does not contribute to $(\Delta\omega_a/\omega_a)$ with terms $\propto|C_a|^2$.

Note that when $\Omega \ll |\omega_d|$, the three-mode interaction always lowers the frequency ω_a [equation (B8)]. On the other hand, the four-mode interaction increases ω_a (as $\eta_{22} < 0$), making $\Delta\omega_a$ 70 per cent smaller than the value predicted using three-mode coupling only. Numerically, we find $\Delta\omega_a/\omega_a \simeq -2.7|C_a|^2$ using the coupling coefficients presented in Table 1. To arrive at these numbers, we note that the Cowling approximation should not be assumed for f-modes as terms due to perturbed gravity could significantly modify the coupling coefficients. We thus extend Weinberg (2016) and show explicitly in Appendix D the expressions for the perturbed gravity terms in η_{abcd}.

In the left panel of Fig. B1, we compare the anharmonic frequency shift (i.e. frequency shift proportional to the energy of the mode) with equation (16). Because $\omega_a/(\omega_a - 2\Omega) \simeq 2$ when $f_{\rm gw} = 1000\,{\rm Hz}$, we have $|C_a| \sim |C_c|$ and thus equation (16) dominates throughout the evolution. On the other hand, it is possible for us to enter the regime where the anharmonicity becomes more significant if $|C_a|$ is enhanced relative to other modes due to NS rotation and/or orbital eccentricity (together with relativistic redshifts; see the discussion in Section 5). We defer to future studies to explore this possibility.

Meanwhile, we also emphasize that the partial cancellation between the three-mode and four-mode coupling terms as illustrated in our discussion on $\Delta\omega_a/\omega_a$ [equations (B8) and (B10)] is in fact a key reason why our analytical result could be accurate with just one iteration of perturbative calculation (Section 2.2). In the right panel of Fig. B1, we compare the evolution of mode energy (top panel) and GW phase shift (bottom panel) with and without four-mode coupling terms. In particular, we obtain the purple curve by setting η_{abcd} to 0 when numerically integrating the differential equations. Note that near the merger, the mode energy runs away unphysically. The reason is illustrated in appendix D of Wu (1998), which we briefly recap below. Consider a toy model where the dynamics of a three-mode system could be describe by a potential Ψ with

$$\Psi = E(A^2 - A^3), \tag{B11}$$

where A corresponds to mode amplitude and $E > 0$ is a constant [cf. equation (43)]. For small oscillations with $|A| \ll 1$, the motion is bound with small corrections from the three-mode interaction. However, if $A \gg 2/3$, the system could climb over the potential well and escape to $A \to \infty$, as seen in the purple curves in Fig. B1. The four-mode interaction stabilizes the system by adding an A^4 piece in the potential.

APPENDIX C: MASS QUADRUPOLE AND LOVE NUMBER

In this appendix, we present the relation between the mass quadrupole tensor and the quadrupole of a mode with angular quantum number (l_a, m_a). This will make the connection between the tidal overlap I_a and the Love number k_2 more transparent. It is also useful for deriving the Burke–Thorne dissipation terms in the differential equations.

We first consider the mass quadrupole of the NS induced by the tide. Focusing on the quadrupole with spherical harmonic degree (l, m) and using a Lagrangian picture with perturbed quantities denoted by the prime symbol, $\boldsymbol{x'} = \boldsymbol{x} + \boldsymbol{\xi}$, we have

$$\begin{aligned} Q^{\rm ns}_{lm} &= \int {\rm d}^3x'\rho(x')x'^l Y^*_{lm}(\theta',\phi') - \int {\rm d}^3x\rho(x)x^l Y^*_{lm}(\theta,\phi), \\ &= \int {\rm d}^3x\rho(x)\left\{\boldsymbol{\xi}\cdot\nabla\left[x^l Y^*_{lm}(\theta,\phi)\right] + \frac{1}{2}\boldsymbol{\xi}\cdot(\boldsymbol{\xi}\cdot\nabla)\nabla\left[x^l Y^*_{lm}(\theta,\phi)\right]\right\}, \\ &= \left(\sum_a^{m_a=m} I_a c_a + \frac{1}{2}\sum_{ab}^{m_a+m_b+m=0} J_{ablm}c^*_a c^*_b\right) MR^l, \end{aligned} \tag{C1}$$

where in the second line we have used $\rho(x'){\rm d}^3x' = \rho(x){\rm d}^3x$ for mass conservation and then expanded $x^l Y^*_{\rm lm}$ around $\boldsymbol{x}$ to second order in $\boldsymbol{\xi}$. Then in the third line, we have first expanded $\boldsymbol{\xi}$ into eigenmodes and then used directly the definition of I_a and J_{ablm}. Note that the first, linear term selects out modes with $(l_a, m_a) = (l, m)$ and the second, non-linear term has contributions from modes with $m_a + m_b + m = 0$, $l_a + l_b + l =$ even, and $|l_a - l_b| \le l \le l_a + l_b$.

To get the quadrupole in the Cartesian coordinate, we follow Poisson & Will (2014) and use the tensor spherical harmonic $\mathcal{Y}$ defined through $Y_{\rm lm}(\theta,\phi) = \mathcal{Y}^{\langle i_1\ldots i_l\rangle *}_{\rm lm} n_{\langle i_1\ldots i_l\rangle}(\theta,\phi)$, where $n_{\langle i_1\ldots i_l\rangle}$ is a tensor formed by unit vectors n^i, with $\boldsymbol{n} = [\sin\theta\cos\phi, \sin\theta\sin\phi, \cos\theta]^T$. The angular bracket denotes taking the STF part. Since the background geometry is Euclidean, we have $n^i = n_i$. This allows us to relate the quadrupole evaluated for a particular spherical harmonic (which is directly obtained from our modal decomposition) to that in the Cartesian coordinate (which is convenient for computing, e.g. the Burke–Thorne terms) as

$$Q^{\langle i_1\ldots i_l\rangle}_{\rm ns} = N_l \sum_m \mathcal{Y}^{\langle i_1\ldots i_l\rangle *}_{lm} Q^{\rm ns}_{lm}, \tag{C2}$$

where $N_l = 4\pi l!/(2l+1)!!$. Note further $\mathcal{Y}^{\langle i_i\ldots i_l\rangle}_{l,-m} = (-1)^m \mathcal{Y}^{\langle i_1\ldots i_l\rangle *}_{\rm lm}$. Restricting to $l = 2$, we have

$$\mathcal{Y}_{22} = \sqrt{\frac{15}{32\pi}}\begin{bmatrix} 1 & -i & 0 \\ -i & -1 & 0 \\ 0 & 0 & 0 \end{bmatrix} \text{ and } \mathcal{Y}_{20} = \sqrt{\frac{5}{16\pi}}\begin{bmatrix} -1 & 0 & 0 \\ 0 & -1 & 0 \\ 0 & 0 & 2 \end{bmatrix}, \tag{C3}$$

together with $N_2 = 8\pi/15$.

We are most interested in the $l = 2$ quadrupole, which can be written as

$$\frac{Q_{\rm ns}^{\langle ij\rangle}}{MR^2} = N_2 \sum_m \left(\sum_{a,\omega_a>0}^{m_a=m} 2{\rm Re}\left[\mathcal{Y}_{2m_a}^{\langle ij\rangle *} I_a c_a\right] + \sum_{ab,\omega_a>0}^{m_a+m_b=-m} {\rm Re}\left[\mathcal{Y}_{2m}^{\langle ij\rangle *} J_{ab2m} c_a^* c_b^*\right] \right). \tag{C4}$$

The first term describes the linear contribution from $l_a = 2$ modes and the second piece corresponds to the non-linear correction (note that a runs over only positive-frequency modes while b runs over both signs of frequencies).

Equation (C4) can be especially helpful for us to see the connection between the modal expansion used in our analysis and the Love number, k_2, which is commonly used by the GW community. Formally, k_2 is defined by

$$Q_{ij}^{\rm ns} = -\frac{2}{3} k_2 R^5 \mathcal{E}_{ij}, \tag{C5}$$

where

$$\mathcal{E}_{ij} = -M' \partial_{ij} \frac{1}{r} \tag{C6}$$

is the tidal potential. We note (Poisson & Will 2014)

$$\partial_{i_1\ldots i_l} \frac{1}{r} = \partial_{\langle i_1\ldots i_l\rangle} \frac{1}{r} = (-1)^l (2l-1)!! \frac{n_{\langle i_1\ldots i_l\rangle}^{\rm orb}}{r^{l+1}}, \tag{C7}$$

and

$$n_{\rm orb}^{\langle i_1\ldots i_l\rangle} = N_l \sum_m \mathcal{Y}_{lm}^{*\,<i_1\ldots i_l>} Y_{lm}^*(\pi/2, \phi) = \sum_m \frac{l!}{(2l-1)!!} W_{lm} e^{-im\phi} \mathcal{Y}_{lm}^*, \tag{C8}$$

where we have used $W_{lm} \equiv 4\pi(2l+1)^{-1} Y_{lm}(\pi/2, 0)$ and the fact that the binary motion is in the $\theta = \pi/2$ plane. Using equation (C4) and grouping terms with the same $\mathcal{Y}_{\rm lm}^{\langle ij\rangle}$, we can find the Love number for each m

$$k_{2m} = \frac{2\pi}{5} \frac{M'}{M} \left(\frac{r}{R}\right)^3 \frac{1}{W_{lm}} \left(\sum_a^{m_a=m} I_a C_a + \frac{1}{2} \sum_{ab}^{m_a+m_b=-m} J_{ab2m} C_a^* C_b^* \right). \tag{C9}$$

One can further plug in the leading-order solution of C_a as described in Sections 2.1 and 2.2 to obtain an effective Love number (for each harmonic m, see also Andersson & Pnigouras 2020; Passamonti et al. 2022). Using the linear, adiabatic solution of C_a, we have

$$k_{2m} = k_2 = \frac{4\pi}{5} \sum_{a,\omega_a>0}^{m_a=m} I_a^2. \tag{C10}$$

Note that in the linear, adiabatic limit, the values of k_{2m} are the same for different ms and can be collectively denoted by a single number k_2. Note further that the summation over modes is strongly dominated by the $l_a = 2$ f-mode (Table 1). Using $I_a = 0.32$, we find $k_2 = 0.26$ in the linear, adiabatic limit, which agrees well with the expected value (Poisson & Will 2014).

The relations summarized in this Appendix will also be useful for computing the Burke–Throne dissipation terms following Flanagan & Hinderer (2008). In particular, the interaction between the orbital and tidal quadrupole modifies the PP Burke–Throne terms in three ways.

First, in equation (6a) of Flanagan & Hinderer (2008), there will be a term arising from the quadrupole of the NS,

$$g_{\rm (gw,ns)}^i = -\frac{2}{5} r_j \frac{d^5}{dt^5} Q_{\rm ns}^{\langle ij\rangle}, \tag{C11}$$

where $\boldsymbol{r} = r\boldsymbol{n}_{\rm orb} = r\,[\cos\phi, \sin\phi, 0]$.

We compute the total quadrupole of the NS in the Cartesian coordinate in terms of each mode's contribution using equation (C4). To evaluate the temporal derivatives of $Q_{\rm ns}^{\langle ij\rangle}$, we note

$$\frac{{\rm d}^5 c_a}{{\rm d}t^5} = \frac{{\rm d}^5}{{\rm d}t^5}[C_a \exp(-im\phi)] \simeq -i(m\Omega)^5 C_a \exp(-im\phi), \tag{C12}$$

$$\frac{{\rm d}^5 (c_a^* c_b^*)}{{\rm d}t^5} = \frac{{\rm d}^5}{{\rm d}t^5}[C_a^* C_b^* \exp(-im\phi)] \simeq -i(m\Omega)^5 C_a^* C_b^* \exp(-im\phi), \tag{C13}$$

where in the second line we have used $m_a + m_b + m = 0$ as required by the angular selection rule. We have dropped terms that are smaller than the dominant one by $\mathcal{O}\left(t_{\rm gw}\dot{\phi}\right)$. Here, $t_{\rm gw} \equiv r/\dot{r}$ is the characteristic time-scale for GW-induced orbital decay. We then convert the Cartesian $f_{\rm gw,ns}^i$ back to spherical coordinates, leading to

$$g_\phi^{\rm (gw,ns)} \simeq -\frac{128}{5}\sqrt{\frac{2\pi}{15}} M R^2 r \Omega^5 \sum_{m=\pm 2} \left(\sum_{a,\omega_a>0}^{m_a=m} I_a {\rm Re}\,[C_a] + \frac{1}{2} \sum_{ab,\omega_a>0}^{m_a+m_b=-m} J_{ab2m} {\rm Re}\,[C_a C_b] \right). \tag{C14}$$

If we use the convention of Section 2.2 and use (a, b, c) to specifically denote the positive-frequency modes with $(m_a, m_b, m_c) = (2, -2, 0)$ and $l_a = l_b = l_c = 2$, we can further simplify the second term in the parentheses as

$$\frac{1}{2} \sum_{m=\pm 2} \sum_{ab,\omega_a>0}^{m_a+m_b=-m} J_{ab2m} {\rm Re}\,[C_a C_b] = 2 J_2 {\rm Re}\,[C_a C_c + C_b C_c] \simeq \frac{4\omega_a^2}{\omega_a^2 - 4\Omega^2} J_2 W_{22} W_{20} \left(\frac{M'}{M}\right)^2 I_a^2 R^6 \frac{\Omega^4}{M_{\rm t}^2}. \tag{C15}$$

Secondly, the tidal back-reaction modifies the derivatives of the orbital quadrupole, defined as

$$Q^{\langle ij\rangle}_{\rm orb} = \mu r^2 n^{\langle ij\rangle}_{\rm orb} = \frac{2}{3}\sum_m W_{2m} Q_{2m} \mathcal{Y}^{\langle ij\rangle *}_{2m}, \tag{C16}$$

where we have used equation (C8) and defined $Q_{2m} = \mu r^2 \exp[-im\phi]$. To compute its derivatives, we keep replacing the derivatives of r, ϕ, and C_a by the conservative parts of their equation of motion (Flanagan & Hinderer 2008),

$$\ddot{r} \to r\dot{\phi}^2 - \tfrac{M+M'}{r^2} + g_r^{\rm (tide)}, \tag{C17}$$

$$r\ddot{\phi} \to -2\dot{r}\dot{\phi} + g_\phi^{\rm (tide)}. \tag{C18}$$

$$\dot{C}_a \to -i(\omega_a - m_a\dot{\phi})C_a + i\omega_a\left[\frac{M'}{M}W_{lm}\left(\frac{R}{r}\right)^{l+1}\left(I_a + \sum_{b,lm} J_{ablm}C^*_b\right) + \sum_{bc}\kappa_{abc}C^*_b C^*_c\right] \tag{C19}$$

Of particular interest is the appearance of the $g_r^{\rm (tide)}$ term [equation (28)], which modifies the $r-\Omega$ relation of the orbit [see also Section 4 and equation (39)]. As a result, in addition to the PP terms given by equations (31) and (32), we need to add additional corrections given by

$$g_\phi^{\rm (gw,br)} \simeq -\frac{96}{5}MM'\left(\frac{R}{r}\right)^2\Omega^3\sum_a^{\omega_a>0}\left[W_{l_a m_a}I_a {\rm Re}[C_a] + \left(\frac{1}{2}\sum_{b,lm}W_{lm}J_{ablm}{\rm Re}[C_a C_b]\right)\right]. \tag{C20}$$

$$g_r^{\rm (gw,br)} \simeq 0 \tag{C21}$$

It is interesting to note that

$$g_\phi^{\rm (gw,pp)} + g_\phi^{\rm (gw,br)} = -\frac{32}{5}\mu r^3\Omega^5, \tag{C22}$$

a form one would intuitively expect. Note that here $r = r(\Omega)$ is given by the modified $r-\Omega$ relation in equation (39).

Lastly, the Burke–Thorne force also acts on the modes. To derive its expression, we can first consider the acceleration $\boldsymbol{a}^{\rm (gw)}$ it induces on a perturbed fluid element at $\boldsymbol{x}' = \boldsymbol{x} + \boldsymbol{\xi}$. First we note that

$$\boldsymbol{a}_{\rm gw}(\boldsymbol{x}') = \boldsymbol{a}_{\rm gw}(\boldsymbol{x}) + \boldsymbol{\xi}\cdot\nabla\boldsymbol{a}_{\rm gw}(\boldsymbol{x}). \tag{C23}$$

Furthermore,

$$a^i_{\rm gw}(\boldsymbol{x}) = -\frac{2}{5}x^j\frac{{\rm d}^5}{{\rm d}t^5}Q^{\langle ij\rangle}_{\rm orb}. \tag{C24}$$

To proceed, we first decompose the orbital quadrupole into tensor spherical harmonics using equation (C16) and note

$$x^j\mathcal{Y}^{\langle ij\rangle *}_{2m} = (x^i x^j)_{;i}\mathcal{Y}^{\langle ij\rangle *}_{2m} = \left(x^2 n^{\langle ij\rangle}\mathcal{Y}^{\langle ij\rangle *}_{2m}\right)_{;i} = (x^2 Y_{2m})_{;i}, \tag{C25}$$

where the semicolon symbol stands for covariant derivative and we have used the identities $n^{ij}\mathcal{Y}^{\langle ij\rangle *}_{2m} = n^{\langle ij\rangle}\mathcal{Y}^{\langle ij\rangle *}_{2m} = Y_{lm}$ (Poisson & Will 2014). We are now ready to write

$$\boldsymbol{a}_{\rm gw}(\boldsymbol{x}') = -\frac{2}{15}\sum_m W_{2m}\left[\nabla\left(x^2Y_{2m}\right) + (\boldsymbol{\xi}\cdot\nabla)\nabla\left(x^2Y_{2m}\right)\right]\frac{{\rm d}^5Q_{2m}}{{\rm d}t^5}. \tag{C26}$$

Its effect on each mode can be obtained by first contracting $\boldsymbol{a}_{\rm gw}$ with $\boldsymbol{\xi}^*$ and then integrating over $\rho{\rm d}^3x$ (Schenk et al. 2002). We thus have (for $l_a = 2$)

$$\dot{c}_a + i\omega_a c_a = i\omega_a\left[(\text{conservative terms}) + Z_a\right], \tag{C27}$$

where

$$Z_a = -\frac{2}{15}W_{2m_a}\frac{R^3}{M}\left(I_a\frac{{\rm d}^5Q_{2m_a}}{{\rm d}t^5} + \sum_b^{m_a+m_b+m=0}J_{ab2m}c^*_b\frac{{\rm d}^5Q^*_{2m}}{{\rm d}t^5}\right). \tag{C28}$$

One can verify that when the non-linear tide piece is ignored, our result reduces to equation (6b) of Flanagan & Hinderer (2008). This can be seen by directly contracting both sides of equation (6b) of Flanagan & Hinderer (2008) with $\mathcal{Y}_{\rm lm}$ and using the identity $\mathcal{Y}^*_{lm'}\mathcal{Y}_{lm} = \delta_{mm'}/N_l$ (Thorne 1980). The result follows by further plugging the linear part of $Q^{\rm ns}_{\rm lm}$ [equation (C1)] into the left-hand side of equation (6b) of Flanagan & Hinderer (2008).

Equation (C22) suggests that we have

$$\frac{{\rm d}^5Q_{2m}}{{\rm d}t^5} \simeq -i(m\Omega)^5\mu r^2 e^{-im\phi}. \tag{C29}$$

We thus have

$$Z_a = \begin{cases} i\frac{2}{15}W_{22}\frac{M'}{M_{\rm t}}\left(\frac{R}{r}\right)^3(m_a r\Omega)^5\left(I_a + \sum_b^{m_b=0}J_{ab2-m_a}c^*_b\right)e^{-im\phi}, & \text{for } m_a = \pm 2, \\ i\frac{2}{15}W_{20}\frac{M'}{M_{\rm t}}\left(\frac{R}{r}\right)^3(m_b r\Omega)^5\left(\sum_b^{m_b=-m=\pm 2}J_{ab2-m_b}C^*_b\right), & \text{for } m_a = 0. \end{cases} \tag{C30}$$

The effect of Z_a is to create an imaginary part in C_a,

$$\mathrm{Im}\,[C_a] \simeq \frac{\omega_a}{\omega_a - m\Omega}\mathrm{Im}\left[Z_a e^{im\phi}\right], \tag{C31}$$

which then leads to a tangential tidal acceleration due to mode a

$$g_\phi^{(\mathrm{gw},a)} \simeq -\frac{4}{15}m_a^6 W_{lm_a}^2 I_a^2 M' R^3 \left(\frac{R}{r}\right)^2 \frac{\omega_a}{\omega_a - m_a\Omega}\Omega^5 + (\text{nonlinear terms}). \tag{C32}$$

We thus see that while $m_a = 2$ and $m_a = -2$ modes have opposite signs for Z_a, their contributions to the orbital decay add coherently. It is also easy to show that the $m_a = 0$ mode does not contribute to the orbital decay via this channel even at the non-linear order we are considering.

Besides terms due to the interaction between tidal and orbital quadrupoles, there is also damping on the f-mode due to its quadrupole beating with itself. This leads to an additional term in Z_a given by

$$Z_a^{(\mathrm{mode})} = -\frac{8\pi}{75}I_a^2 R^5 \frac{d^5 c_a}{dt^5} \simeq i\frac{8\pi}{75}W_{l_a m_a} I_a^3 \frac{M'}{M}\left(\frac{R}{r}\right)^3 \frac{\omega_a}{\omega_a - m_a\Omega}(m_a R\Omega)^5. \tag{C33}$$

This term is smaller than equation (37) by a factor of $\mathcal{O}(R/r)^5$, which is smaller than the leading-order non-linear effects we consider that corrects the linear solution at the $(R/r)^3$ order. We thus ignore its effect in our discussions. None the less, this term can be amplified if the mode is close to resonance with the orbit due to NS rotation and/or orbital eccentricity. See the discussions in Section 5.

APPENDIX D: FOUR-MODE COUPLING WITHOUT THE COWLING APPROXIMATION

We can break the four-mode coupling into seven pieces (Van Hoolst 1994)

$$\eta_{abcd} = -\frac{\mathrm{I} + \mathrm{II} + \mathrm{III} + \mathrm{IV} + \mathrm{V} + \mathrm{VI} + \mathrm{VII}}{6E_0}, \tag{D1}$$

where terms I-V are provided in appendix C Weinberg (2016). Here, we compute terms VI and VII that are due to perturbed gravity. For the coupling among f-modes, we find that the perturbed gravity terms (VI and VII) are crucial as they can modify the results obtained under the Cowling approximation by $\sim 70\%$. In this appendix specifically, we will use r to denote the radial coordinate of a fluid element inside the NS. It should not be confused with the orbital separation as we will consider only an isolated NS here.

The first perturbed gravity term we need to evaluate is,

$$\begin{aligned}\mathrm{VI} = -\int \mathrm{d}^3x\rho \Bigg[&\xi_a^i\xi_b^j\left(\int \mathrm{d}^3x'\rho(x')\xi_c^{k'}\xi_d^{s'}|\boldsymbol{x}-\boldsymbol{x'}|^{-1}_{;k's'}\right)_{;ij} + \\ &+ \xi_a^i\xi_c^j\left(\int \mathrm{d}^3x'\rho(x')\xi_b^{k'}\xi_d^{s'}|\boldsymbol{x}-\boldsymbol{x'}|^{-1}_{;k's'}\right)_{;ij} + \xi_a^i\xi_d^j\left(\int \mathrm{d}^3x'\rho(x')\xi_b^{k'}\xi_c^{s'}|\boldsymbol{x}-\boldsymbol{x'}|^{-1}_{;k's'}\right)_{;ij}\Bigg],\end{aligned} \tag{D2}$$

where ';' stands for covariant derivative and a quantity with a primed index means that it is evaluated with respect to $\boldsymbol{x}'$. We can expand

$$\frac{1}{|\boldsymbol{x}-\boldsymbol{x}'|} = \sum_{lm}\tilde{r}_l(x,x')Y_{lm}^*(\theta',\phi')Y_{lm}(\theta,\phi), \tag{D3}$$

where

$$\tilde{r}_l(r,r') = \frac{4\pi}{2l+1}\times\begin{cases}\frac{r'^l}{r^{l+1}} & \text{if } r'\le r,\\ \frac{r^l}{r'^{l+1}} & \text{if } r'>r.\end{cases} \tag{D4}$$

Following Weinberg et al. (2012), we use a covariant basis with vectors $\epsilon_i = h_i e_i$, where $h_r = 1$, $h_\theta = r$, $h_\phi = r\sin\theta$, and $e_{r,\theta,\phi}$ are unit vectors along the r,θ,ϕ directions. The non-zero components of the metric are $(g_{rr}, g_{\theta\theta}, g_{\phi\phi}) = (1, r^2, r^2\sin^2\theta)$. The Lagrangian displacement vector for an eigenmode can be written as[5]

$$\boldsymbol{\xi}_a = \left[\xi_a^r, \xi_a^\theta, \xi_a^\phi\right] = \left[a_r Y_a, \frac{a_h}{r}\frac{\partial Y_a}{\partial\theta}, \frac{a_h}{r\sin^2\theta}\frac{\partial Y_a}{\partial\phi}\right], \tag{D5}$$

where $Y_a \equiv Y_{l_a,m_a}$.

Consider a specific harmonic and focus on the inner integral first (i.e. primed coordinate). We have terms like (in the right-hand side, all terms are evaluated in the primed coordinate)

$$\xi_c^{r'}\xi_d^{r'}(\tilde{r}_l Y_{lm}^*)_{;r'r'} = c_r d_r\left(\tfrac{\partial^2}{\partial r'^2}\tilde{r}_l\right)Y_c Y_d Y_{lm}^*, \tag{D6}$$

$$\xi_c^{r'}\xi_d^{\theta'}(\tilde{r}_l Y_{lm}^*)_{;r'\theta'} = c_r d_h\left(\tfrac{1}{r'}\tfrac{\partial\tilde{r}_l}{\partial r'} - \tfrac{\tilde{r}_l}{r'^2}\right)Y_c\tfrac{\partial Y_d}{\partial\theta'}\tfrac{Y_{lm}^*}{\partial\theta'}, \tag{D7}$$

[5]Note that we use ξ_a^i to indicate the i component of $\boldsymbol{\xi}_a$. In the coordinate we consider, the coordinate index corresponds to $i = (r,\theta,\phi)$. On the other hand, we use a_r and a_h to indicate the radial and tangential component of the Lagrangian displacement and the subscripts r and h do not corresponds to coordinate indices.

$$\xi_c^{r'}\xi_d^{\phi'}(\tilde{r}_l Y_{lm}^*)_{;r'\phi'} = c_r d_h \left(\frac{1}{r'}\frac{\partial\tilde{r}_l}{\partial r'} - \frac{\tilde{r}_l}{r'^2}\right)\frac{Y_c}{\sin^2\theta'}\frac{\partial Y_d}{\partial\phi'}\frac{\partial Y_{lm}^*}{\partial\phi'}, \tag{D8}$$

$$\xi_c^{\theta'}\xi_d^{\theta'}(\tilde{r}_l Y_{lm}^*)_{;\theta'\theta'} = c_h d_h \left(\frac{\tilde{r}_l}{r'^2}\frac{\partial Y_c}{\partial\theta'}\frac{\partial Y_d}{\partial\theta'}\frac{\partial Y_{lm}^*}{\partial\theta'^2} + \frac{1}{r'}\frac{\partial\tilde{r}_l}{\partial r'}\frac{\partial Y_c}{\partial\theta'}\frac{\partial Y_d}{\partial\theta'}Y_{lm}^*\right), \tag{D9}$$

$$\xi_c^{\theta'}\xi_d^{\phi'}(\tilde{r}_l Y_{lm}^*)_{;\theta'\phi'} = c_h d_h \frac{\tilde{r}_l}{r'^2}\frac{1}{\sin^2\theta'}\frac{\partial Y_c}{\partial\theta'}\frac{\partial Y_d}{\partial\phi'}\left(\frac{\partial^2 Y_{lm}^*}{\partial\theta'\partial\phi'} - \frac{\cos\theta'}{\sin\theta'}\frac{\partial Y_{lm}^*}{\partial\phi'}\right), \tag{D10}$$

$$\xi_c^{\phi'}\xi_d^{\phi'}(\tilde{r}_l Y_{lm}^*)_{;\phi'\phi'} = c_h d_h \frac{\partial Y_c}{\partial\phi'}\frac{\partial Y_d}{\partial\phi'}\left(\frac{\tilde{r}_l}{r'^2}\frac{1}{\sin^4\theta'}\left(\frac{\partial^2 Y_{lm}^*}{\partial\phi'^2} + \sin\theta'\cos\theta'\frac{\partial Y_{lm}^*}{\partial\theta}\right) + \frac{1}{r'}\frac{\partial\tilde{r}_l}{\partial r'}\frac{1}{\sin^2\theta'}Y_{lm}^*\right). \tag{D11}$$

Thus

$$\int \mathrm{d}^3x'\rho(x')c^{k'}d^{s'}|\boldsymbol{x}-\boldsymbol{x}'|^{-1}_{;k's'} = \sum_l^{m=m_c+m_d}(-1)^m\frac{4\pi}{2l+1}Y_{\mathrm{lm}}(\theta,\phi)\left[\mathrm{VI}_{cd}^{<r}(r)+\mathrm{VI}_{cd}^{>r}(r)\right], \tag{D12}$$

where we have used $Y_{\mathrm{lm}}^* = (-1)^m Y_{l-m}$, and the angular selection role requires $m = m_c + m_d = -(m_a + m_b)$. The radial part is defined as

$$\begin{aligned}\mathrm{VI}_{cd}^{<r}(r) = r^{-(l+1)}\int_0^r \mathrm{d}r' r'^l\rho(r')\big[&l(l-1)c_{r'}d_{r'}T_{cdl-m} + (l-1)c_{r'}d_{h'}F_{c,dl-m} + (l-1)c_{h'}d_{r'}F_{d,cl-m}\\ &+ c_{h'}d_{h'}\left(G_{l-m,cd} + lF_{l-m,cd}\right)\big],\end{aligned} \tag{D13}$$

$$\begin{aligned}\mathrm{VI}_{cd}^{>r}(r) = r^{l}\int_r^R \mathrm{d}r' r'^{-(l+1)}\rho(r')\big[&(l+1)(l+2)c_{r'}d_{r'}T_{cdl-m} - (l+2)c_{r'}d_{h'}F_{c,dl-m} - (l+2)c_{h'}d_{r'}F_{d,cl-m}\\ &+ c_{h'}d_{h'}\left(G_{l-m,cd} - (l+1)F_{l-m,cd}\right)\big].\end{aligned} \tag{D14}$$

We further define $\mathrm{VI}_{cd}(r) = \mathrm{VI}_{cd}^{<r}(r) + \mathrm{VI}_{cd}^{>r}(r)$. The angular parts have been integrated following Weinberg et al. (2012)

$$T_{abc} = \int \mathrm{d}\Omega Y_a Y_b Y_c, \tag{D15}$$

$$F_{a,bc} = \int \mathrm{d}\Omega Y_a \nabla^i Y_b \nabla_j Y_c = \frac{T_{abc}}{\Lambda_b^2+\Lambda_c^2-\Lambda_a^2}, \tag{D16}$$

$$G_{a,bc} = \int \mathrm{d}\Omega g^{ik}g^{js}\nabla_i\nabla_j Y_a \nabla_k Y_b \nabla_s Y_c = \frac{T_{abc}}{4}[\Lambda_a^4 - (\Lambda_b^2-\Lambda_c^2)^2], \tag{D17}$$

where $\Lambda_a^2 = l_a(l_a+1)$. Paired subscripts not separated by a comma are symmetric in those indices.

The outer integral can be evaluated similarly,

$$\begin{aligned}&\int \mathrm{d}^3x\rho\xi_a^i\xi_b^j\left(\int \mathrm{d}^3x'\rho(x')\xi_c^{k'}\xi_d^{s'}|\boldsymbol{x}-\boldsymbol{x}'|^{-1}_{;k's'}\right)_{;ij}\\ &= \sum_l^{m=m_c+m_d}(-1)^m\frac{4\pi}{2l+1}\int \mathrm{d}x^3\rho\xi_a^i\xi_b^j\left[\mathrm{VI}_{cd}(r)Y_{lm}\right]_{;ij}\\ &= \sum_l^{m=m_c+m_d}(-1)^m\frac{4\pi}{2l+1}\int \mathrm{d}r r^2\rho(r)\left[a_r b_r\left(\frac{\partial^2\mathrm{VI}_{cd}}{\partial r^2}\right)T_{ablm} + a_r b_h\left(\frac{1}{r}\frac{\partial\mathrm{VI}_{cd}}{\partial r} - \frac{\mathrm{VI}_{cd}}{r^2}\right)F_{a,blm} + a_h b_r\left(\frac{1}{r}\frac{\partial\mathrm{VI}_{cd}}{\partial r} - \frac{\mathrm{VI}_{cd}}{r^2}\right)F_{b,alm}\right.\\ &\quad\left. + a_h b_h\left(\frac{\mathrm{VI}_{cd}}{r^2}G_{lm,ab} + \frac{1}{r}\frac{\partial\mathrm{VI}_{cd}}{\partial r}F_{lm,ab}\right)\right].\end{aligned} \tag{D18}$$

The other perturbed gravity term we need to evaluate is

$$\mathrm{VII} = \int \mathrm{d}^3x\rho\left[\xi_a^i\xi_b^j\xi_c^k\delta\Phi_{d;ijk} + \xi_a^i\xi_b^j\xi_d^k\delta\Phi_{c;ijk} + \xi_a^i\xi_c^j\xi_d^k\delta\Phi_{b;ijk} + \xi_b^i\xi_c^j\xi_d^k\delta\Phi_{a;ijk}\right], \tag{D19}$$

where $\delta\Phi_d$ is the Eulerian perturbation of the gravitational potential induced by mode d and it is given by $\delta\Phi_d(r,\theta,\phi) = \delta\phi_d(r)Y_d(\theta,\phi)$.

We will have terms

$$(\delta\phi_d Y_d)_{;rrr} = \frac{\partial^3\delta\phi_d}{\partial r^3}Y_d, \tag{D20}$$

$$(\delta\phi_d Y_d)_{;rr\theta} = \left(\frac{\partial^2\delta\phi_d}{\partial r^2} - \frac{2}{r}\frac{\partial\delta\phi_d}{\partial r} + \frac{2}{r^2}\delta\phi_d\right)\frac{\partial Y_d}{\partial\theta} \tag{D21}$$

$$(\delta\phi_d Y_d)_{;rr\phi} = \left(\frac{\partial^2\delta\phi_d}{\partial r^2} - \frac{2}{r}\frac{\partial\delta\phi_d}{\partial r} + \frac{2}{r^2}\delta\phi_d\right)\frac{\partial Y_d}{\partial\phi} \tag{D22}$$

$$(\delta\phi_d Y_d)_{;r\theta\theta} = r\frac{\partial^2\delta\phi_d}{\partial r^2}Y_d + \frac{\partial\delta\phi_d}{\partial r}\left(\frac{\partial^2 Y_d}{\partial\theta^2} - Y_d\right) - \frac{2}{r}\delta\phi_d\frac{\partial^2 Y_d}{\partial\theta^2} \tag{D23}$$

$$(\delta\phi_d Y_d)_{;r\theta\phi} = \frac{\partial\delta\phi_d}{\partial r}\left(\frac{\partial^2 Y_d}{\partial\theta\partial\phi} - \frac{\cos\theta}{\sin\theta}\frac{\partial Y_d}{\partial\phi}\right) + \frac{2\delta\phi_d}{r}\left(-\frac{\partial^2 Y_d}{\partial\theta\partial\phi} + \frac{\cos\theta}{\sin\theta}\frac{\partial Y_d}{\partial\phi}\right) \tag{D24}$$

$$(\delta\phi_d Y_d)_{;r\phi\phi} = r\frac{\partial^2\delta\phi_d}{\partial r^2}\sin^2\theta Y_d + \frac{\partial\delta\phi_d}{\partial r}\left(\frac{\partial^2 Y_d}{\partial\phi^2} + \sin\theta\cos\theta\frac{\partial Y_d}{\partial\theta} - \sin^2\theta Y_d\right) - \frac{2\delta\phi_d}{r}\left(\frac{\partial^2 Y_d}{\partial\phi^2} + \sin\theta\cos\theta\frac{\partial Y_d}{\partial\theta}\right) \tag{D25}$$

$$(\delta\phi_d Y_d)_{;\theta\theta\theta} = 3r\frac{\delta\phi_d}{\partial r}\frac{\partial Y_d}{\partial\theta} + \delta\phi_d\left(\frac{\partial^3 Y_d}{\partial\theta^3} - 2\frac{\partial Y_d}{\partial\theta}\right) \tag{D26}$$

$$(\delta\phi_d Y_d)_{;\theta\theta\phi} = r\frac{\partial\delta\phi_d}{\partial r}\frac{\partial Y_d}{\partial\phi} + \delta\phi_d\left(\frac{\partial^3 Y}{\partial\theta^2\partial\phi} - 2\frac{\cos\theta}{\sin\theta}\frac{\partial^2 Y}{\partial\theta\partial\phi} + 2\frac{\cos^2\theta}{\sin^2\theta}\frac{\partial Y}{\partial\phi}\right) \tag{D27}$$

$$(\delta\phi_d Y_d)_{;\theta\phi\phi} = r\frac{\partial\delta\phi_d}{\partial r}\sin^2\theta\frac{\partial Y}{\partial\theta} + \delta\phi_d\left(\frac{\partial^3 Y_d}{\partial\theta\partial^2\phi} + \sin\theta\cos\theta\frac{\partial^2 Y}{\partial\theta^2} - 2\frac{\cos\theta}{\sin\theta}\frac{\partial^2 Y}{\partial\phi^2} - \frac{\partial Y_d}{\partial\theta}\right) \tag{D28}$$

$$(\delta\phi_d Y_d)_{;\phi\phi\phi} = 3r\frac{\partial\delta\phi_d}{\partial r}\sin^2\theta\frac{\partial Y}{\partial\phi} + \delta\phi_d\left(\frac{\partial^3 Y_d}{\partial\phi^3} + 3\sin\theta\cos\theta\frac{\partial^2 Y_d}{\partial\theta\partial\phi} - 2\frac{\partial Y_d}{\partial\phi}\right). \tag{D29}$$

Because the background is Euclidean, covariant derivatives commute and the results are symmetric with respect to permutations of indices. Thus,

$$\int d\Omega\xi^i_a\xi^j_b\xi^k_c\delta\Phi_{d;ijk}$$

$$= a_r b_r c_r\frac{\partial^3\delta\phi_d}{\partial r^3}T_{\rm abcd} \tag{D30}$$

$$+\Big[a_r b_r c_h F^{(2)}_{ab,cd} + a_r b_h c_r F^{(2)}_{ac,bd} + a_h b_r c_r F^{(2)}_{bc,ad}$$

$$+a_r b_h c_h F^{(2)}_{ad,bc} + a_h b_r c_h F^{(2)}_{bd,ac} + a_h b_h c_r F^{(2)}_{cd,ab}\Big]\frac{1}{r}\frac{\partial^2\delta\phi_d}{\partial r^2} \tag{D31}$$

$$+\Big[-2a_r b_r c_h F^{(2)}_{ab,cd} - 2a_r b_h c_r F^{(2)}_{ac,bd} - 2a_h b_r c_r F^{(2)}_{bc,ad}$$

$$+a_r b_h c_h\left(S_{a,bc,d} - (\Lambda^2_d+1)F^{(2)}_{ad,bc}\right) + a_h b_r c_h\left(S_{b,ac,d} - (\Lambda^2_d+1)F^{(2)}_{bd,ac}\right) + a_h b_h c_r\left(S_{c,ab,d} - (\Lambda^2_d+1)F^{(2)}_{cd,ab}\right)$$

$$+a_h b_h c_h\left(G^{(22)}_{ab,cd} + G^{(22)}_{ac,bd} + G^{(22)}_{ad,bc}\right)\Big]\frac{1}{r^2}\frac{\partial\delta\phi_d}{\partial r} \tag{D32}$$

$$+\Big[2a_r b_r c_h F^{(2)}_{ab,cd} + 2a_r b_h c_r F^{(2)}_{ac,bd} + 2a_h b_r c_r F^{(2)}_{bc,ad}$$

$$-2a_r b_h c_h\left(S_{a,bc,d} - \Lambda^2_d F^{(2)}_{ad,bc}\right) - 2a_h b_r c_h\left(S_{b,ac,d} - \Lambda^2_d F^{(2)}_{bd,ac}\right) - 2a_h b_h c_r\left(S_{c,ab,d} - \Lambda^2_d F^{(2)}_{cd,ab}\right)$$

$$+a_h b_h c_h R_{abc,d}\Big]\frac{\delta\phi_d}{r^3}, \tag{D33}$$

where we have defined the following angular integrals (Weinberg 2016),

$$f^{(1)}_{ab} = Y_a Y_b,\ f^{(2)}_{ab} = \nabla Y_a\cdot\nabla Y_b,\ f^{(3)}_{ab} = \nabla_i\nabla^j Y_a\nabla_j\nabla^i Y_b, \tag{D34}$$

$$F^{(i)}_{ab,cd} = \int {\rm d}\Omega Y_a Y_b f^{(i)}_{cd}, \tag{D35}$$

$$G^{(i)}_{ab,cd} = \int {\rm d}\Omega f^{(i)}_{ab} f^{(i)}_{cd}, \tag{D36}$$

$$S_{a,bc,d} = \int {\rm d}\Omega Y_a\nabla_i Y_b\nabla^j Y_c\nabla_j\nabla^i Y_d + \Lambda^2_d F^{(2)}_{ad,bc}, \tag{D37}$$

together with a new integral we introduce in this work,

$$R_{abc,d} = \int {\rm d}\Omega\nabla^i Y_a\nabla^j Y_b\nabla^k Y_c\nabla_i\nabla_j\nabla_k Y_d. \tag{D38}$$

This paper has been typeset from a TEX/LATEX file prepared by the author.